

**EFFECT OF LANTHANUM SUBSTITUTION ON THE
STRUCTURAL, MAGNETIC AND TRANSPORT
PROPERTIES OF Cu-Zn FERRITES**

**M.Sc. Thesis
BY
KAMRUN NAHAR**



**DEPARTMENT OF PHYSICS
KHULNA UNIVERSITY OF ENGINEERING & TECHNOLOGY
KHULNA - 9203, BANGLADESH**

NOVEMBER- 2018

**EFFECT OF LANTHANUM SUBSTITUTION ON THE
STRUCTURAL, MAGNETIC AND TRANSPORT
PROPERTIES OF Cu-Zn FERRITES**

M.Sc. Thesis

BY

KAMRUN NAHAR

ROLL NO. 1755501

SESSION: JANUARY-2017

A THESIS SUBMITTED TO THE DEPARTMENT OF PHYSICS,
KHULNA UNIVERSITY OF ENGINEERING & TECHNOLOGY,
KHULNA - 9203 IN PARTIAL FULFILMENT OF THE
REQUIREMENT FOR THE DEGREE OF MASTER OF SCIENCE



DEPARTMENT OF PHYSICS
KHULNA UNIVERSITY OF ENGINEERING & TECHNOLOGY
KHULNA - 9203, BANGLADESH

NOVEMBER- 2018

Dedicated
to
My
Beloved Parents

DECLARATION

This is to certify that the thesis work entitled as “**Effect of Lanthanum Substitution on the Structural, Magnetic and Transport Properties of Cu-Zn Ferrites**” has been carried out in partial fulfillment of the requirement for M.Sc. degree in the Department of Physics, Khulna University of Engineering & Technology, Khulna-9203, Bangladesh. The above research work or any part of this work has not been submitted to anywhere for the award of any degree or diploma. No other person’s work has been used without due acknowledgement.

Supervisor



.....
Prof. Dr. Shibendra Shekher Sikder

Candidate



.....
KamrunNahar

**KHULNA UNIVERSITY OF ENGINEERING & TECHNOLOGY
DEPARTMENT OF PHYSICS**

Approval

This is to certify that the thesis submitted by *Kamrun Nahar* entitled “Effect of Lanthanum Substitution on the Structural, Magnetic and Transport Properties of Cu-Zn Ferrites” has been accepted by the Board of Examiners for the partial fulfillment of the requirements for the degree of M. Sc. in the Department of Physics, Khulna University of Engineering & Technology, Khulna, Bangladesh on 28 November 2018.

Board of Examiners

Sl. No. Name, Designation & Address

1. Prof. Dr. Shibendra Shekher Sikder
Department of Physics
Khulna University of Engineering & Technology


.....
Chairman & Supervisor

2. Head
Department of Physics
Khulna University of Engineering & Technology


.....
Member

3. Prof. Dr. Md. Mahbub Alam
Department of Physics
Khulna University of Engineering & Technology


.....
Member

4. Prof. Dr. Md. Abdullah Elias Akhter
Department of Physics
Khulna University of Engineering & Technology


.....
Member

5. Dr. Md. Abdul Gafur
Principal Scientific Officer
Bangladesh Council of Scientific and Industrial Research
Dhanmondi, Dhaka-1205


.....
Member
(External)

Acknowledgements

I express all my admiration to Almighty Allah, the merciful, the sustainer and the controller of the universe who has enabled me to submit this humble work leading to the M.Sc. degree.

First and foremost, I would like to express my deep sense of sincere gratitude to my reverend supervisor **Professor Dr. Shibendra Shekher Sikder**, Department of Physics, Khulna University of Engineering & Technology (KUET) for his continuous guidance, excellent cooperation, fruitful comments, suggestion and encouragement for the completion of the research work in a proper and smooth way and of course I convey my heartfelt thanks to his for introducing me to the exciting field of Solid State Physics.

I pay my profound reverence and gratitude to **Professor Dr. Md. Mahbub Alam**, Head, Department of Physics, KUET, for his encouragement, inspiration, and indispensable guidance for my perseverance in research.

I am grateful to **Dr. S. Manjura Hoque**, Head & Chief Scientific Officer, Materials Science Division (MSD), Atomic Energy Centre, Dhaka (AECD) for providing kind opportunity to use the laboratory for experimental work. My thanks are also for **Dr. Mohammed Nazrul Islam Khan**, Principal Scientific Officer (PSO), MSD, AECD, for providing necessary ideas about this research. His valuable direction, suggestions and continuous assessment on work made me conscious and sincere to obtain better results in all experiments.

My special thanks to **Mr. Alamgir Hossain** (Assistant Professor), Department of Physics, KUET, for his support, suggestions and provisions that benefited me much in the completion of this thesis work. I place on record my special gratitude and thanks to **Probal Roy** (Lecturer), Department of Physics, KUET, for his sincere and valuable guidance, suggestions and encouragement extended to me. Without their help and support it was quite difficult to do the research in laboratory.

I am also grateful to **Professor Dr. Md. Abdullah Elias Akhter**, Department of Physics, KUET, **Professor Dr. Joly Sultana**, Department of Physics, KUET, **Md. Kamrul Hasan Reza** (Associate Professor), Department of Physics, KUET, for their support and precious words of encouragement.

My thanks are also for **Mr. Sujit Kumar Shil** (Assistant Professor), **Sumon Deb-Nath** (Assistant Professor), **Suman Halder** (Assistant Professor) and **Saifullah**

(Lecturer), Department of Physics, KUET for their sincere and valuable guidance and encouragement extended to me.

Special thanks to **Subroto Subon Acharjee, Deloar Hossain, Sharmin Akter** and **Al-Masud** for providing their kind help throughout this work.

I am proud to remember my beloved parents, brother and sister for their immeasurable sacrifices, blessings and continuous inspirations throughout my personal life and academic career. I am very much thankful to my friends and my co-workers for their continuous inspirations throughout my thesis work and academic life in Department of Physics, Khulna University of Engineering & Technology (KUET).

My thanks due to Director, Atomic Energy Centre, Dhaka for his kind permission to use the laboratory of Materials Science Division, Atomic Energy Centre, Dhaka to complete my research.

I also wish to thank the authority of Khulna University of Engineering & Technology (KUET), for providing me with the necessary permission and financial assistance for conducting this thesis work.

Kamrun Nahar

Abstract

This thesis work is acquainted with the study of lanthanum (La) doped Cu-Zn ferrite. The composition of the sample is $\text{Cu}_{0.15}\text{Zn}_{0.85}\text{La}_x\text{Fe}_{2-x}\text{O}_4$ where it was prepared for $x = 0.00, 0.02, 0.04, 0.06$ and 0.08 content of La by Solid State Reaction method. The samples were pre-sintered at 800°C for 3 hours and sintered at 1150°C for 3 hours. The substitution of La for various ratio have remarkable effects on the structural, magnetic and electrical properties of Cu-Zn ferrite. The phase identification has carries out by using X-ray diffraction (XRD). The XRD analysis revealed that undoped in Cu-Zn ferrite shows formulation of cubic single phase (fcc) spinel structure without any impurity peak but other four La doped Cu-Zn ferrites are shows additional peaks manifested the formation of secondary phase presumably LaFeO_3 . The values of lattice parameter have the trend of increasing with the increase of x . The bulk density also has a trend of increasing with the increase of La content where the X-ray density decreases. In morphological study, SEM image exhibit uniform surface morphology with well defined spherical grain. The average grain size was calculated using Image J Software and it was observed that, the average grain size decreases with increasing La content. The magnetic properties were studied by investigating M-H curves that was obtained by vibrating sample magnetometer (VSM). The magnetic properties demonstrated a strong dependence of the variation of x . With the increase of x , saturation magnetization (M_s) decreases while remanent magnetization (M_r) and coercivity (H_c) increases. The hysteresis curve for samples of various ratio of La showed the ferromagnetic behavior. The decrease of M_s with increasing of La substitutions has been explained as the effect of dilution of Fe^{3+} magnetic moment by nonmagnetic La^{3+} . The complex permeability, loss tangent, dielectric properties were investigated as a function of frequency upto 120MHz by using impedance analyzer. The initial permeability slightly increases with the increase of La substitution while imaginary permeability decreases. Moreover the dielectric constant decreases rapidly with the increase in frequency at lower frequencies and slowly at higher frequency and almost constant exhibiting normal behavior of ferrites. Dielectric constant decreases with increases of La content in Cu-Zn ferrites. The electrical DC resistivity has a trend of increasing with the increase of La content. The variation of electrical and dielectric in La doped Cu-Zn ferrites are explained on the basis of $\text{Fe}^{2+}/\text{Fe}^{3+}$ ionic concentration with affect La ions as well as the electronic hopping frequency between Fe^{2+} and Fe^{3+} ion.

Contents

	Page No.
Title Page	
Declaration Page	i
Acknowledgement	ii
Abstract	iv
Contents	v
List of Figures	viii
List of Tables	ix
List of Symbols	xi

CHAPTER - I

INTRODUCTION

1.1	Introduction	1
1.2	The Aims and Objectives of the Recent Work	3
1.3	Experimental Reason for this Research Work	4
1.4	Importance of Ferrites	5
1.5	Review of the Earlier Research Work	6
1.6	Outline of the Thesis	8

CHAPTER - II

THEORETICAL BACKGROUND

2.1	Overview of Rare Earth Ferrites	9
2.2	Ferrites	10
2.2.1	Types of Ferrites	11
2.2.2	Spinel Ferrites	12
2.2.3	Cubic Ferrites Garnets	13
2.2.4	Ortho-ferrites	14
2.2.5	Hexagonal ferrites	14
2.3	Types of Spinel Ferrites	15
2.3.1	Cation Distribution in Spinels	15
2.4	Soft Ferrites	16
2.5	Hard Ferrites	17
2.6	Magnetization Process	18

2.6.1	Magnetization Curve	18
2.7	Theory of Initial Permeability	19
2.8	Dielectric Constant	20
2.8.1	Dependence of Dielectric Constant on Frequency	21
2.9	DC Resistivity of Ferrites	21
2.10	Microstructure	22

CHAPTER-III

EXPERIMENTAL PROCEDURE

3.1	Rare Earth Ferrite Preparation	24
3.2	Composition of the Studied Ferrites	24
3.3	Sample Preparation Technique	24
3.3.1	Solid State Reaction Method	25
3.4	Sample Preparation	26
3.4.1	Calculation for Sample Preparation	26
3.4.2	Mixed and Milled the Samples	27
3.4.3	Pre-sintering the Mixture to Form Ferrite	28
3.4.4	Pressing or Extrusion	29
3.4.5	Sintering	30
3.4.6	KSL-1700X-S Furnace	31
3.4.7	Illustration of Temperature Segment Setting for Sintering	32
3.5	Sample Preparation at a Glance	33
3.6	X-ray Diffraction	34
3.6.1	Different Parts of the PHILIPS X' Pert PRO XRD System	35
3.6.2	Interpretation of the XRD data	36
3.6.3	Lattice Parameter	36
3.6.4	X-ray Density and Bulk Density	37
3.6.5	Porosity	37
3.7	Surface Morphology and Microstructure	38
3.7.1	Scanning Electron Microscope (SEM)	38
3.8	Vibrating Sample Magnetometer (VSM)	39
3.8.1	Working Procedure of Vibrating Sample Magnetometer (VSM)	40
3.9	Permeability Measurement	41

3.9.1 Wayne Kerr Precision Impedance Analyzer	41
3.9.2 Permeability	42
3.10 Dielectric Properties	43
3.10.1 Dielectric Constant	44
3.10.2 Dielectric Loss	45
3.11 DC Resistivity	45

CHAPTER-IV

RESULTS AND DISCUSSION

4.0 Introduction	46
4.1 X-ray Diffraction Analysis	46
4.1.1 Phase Analysis	47
4.1.2 Lattice Parameters	48
4.1.3 Density and Porosity	50
4.2 Microstructures of $\text{Cu}_{0.15}\text{Zn}_{0.85}\text{La}_x\text{Fe}_{2-x}\text{O}_4$ Ferrites	52
4.3 Magnetic Properties	54
4.3.1 Hysteresis Loop Analysis	54
4.3.2 Frequency Dependence of Complex Permeability	55
4.3.3 Frequency Dependence of Quality Factor	60
4.4 Frequency Dependent Dielectric Properties	61
4.5 Effect of Ytterbium Substitution on Resistivity	64

CHAPTER-V

CONCLUSIONS

5.1 Conclusions	66
5.2 Scope for Future Work	67
References	68
Conference Publications	73

List of Figures

Figure No.	Descriptions	Page no.
Figure 2.1	Classification of Ferrites	11
Figure 2.2	Crystal Structure of spinel ferrite	12
Figure 2.3	Cubic ferrite of garnet	13
Figure 2.4	Crystal structure of hexagonal ferrite	14
Figure 2.5	(a) Soft Ferrite, (b) Hard Ferrite	17
Figure 2.6	Domain dynamics during various parts of the magnetization curve	18
Figure 2.7	Schematic illustration of capacitive cell	20
Figure 2.8	Porosity character: (a) intergranular, (b) intragranular	23
Figure 2.9	Grain growth (a) discontinuous, (b) duplex (schematic).	23
Figure 3.1	Raw materials in agate mortar with pestle	28
Figure 3.2	Furnace (KSL-1700X made in USA) in the solid state physics laboratory, (KUET).	28
Figure 3.3	Hydraulic press and dies for preparing sample	29
Figure 3.4	Illustration of the stages in sintering of powder particles	31
Figure 3.5	High Temperature Muffle Furnace (KSL-1700X-S) at Solid State Physics Laboratory, KUET	31
Figure 3.6	Graphical presentation of temperature control program segments	32
Figure 3.7	Bragg diffraction of x-rays from successive planes of atoms	34
Figure 3.8	Internal arrangement of a PHILIPS X' Pert PRO X-ray diffractometer	35
Figure 3.9	Porosity	38
Figure 3.10	Scanning Electron Microscope (SEM)	39
Figure 3.11	Vibrating Sample Magnetometer	39
Figure 3.12	Block diagram of vibrating sample magnetometer	41
Figure 3.13	Wayne Kerr Impedance analyzer (6500B series) in Solid State Laboratory, Physics, KUET	41
Figure 3.14	Complex permeability measurement by Wayne Kerr Precision Impedance analyzer	42

Figure 3.15	Schematic arrangement on the silver pasted pellet sample	45
Figure 4.1	X-ray diffraction spectra of $\text{Cu}_{0.15}\text{Zn}_{0.85}\text{La}_x\text{Fe}_{2-x}\text{O}_4$, [where $x = 0.00, 0.02, 0.04, 0.06$ and 0.08] ferrites sintered at 1150°C for 3 hours holding time	47
Figure 4.2	Variation of lattice parameter 'a' with N-R function and determination of exact lattice parameter 'a' of $\text{Cu}_{0.15}\text{Zn}_{0.85}\text{La}_x\text{Fe}_{2-x}\text{O}_4$ ferrites	49
Figure 4.3	Variation of lattice parameters with the increase of La content	50
Figure 4.4	Variation of bulk density and X-ray density as a function of La content	51
Figure 4.5	Variation of SEM micrographs with La contents (x) of $\text{Cu}_{0.15}\text{Zn}_{0.85}\text{La}_x\text{Fe}_{2-x}\text{O}_4$ ferrites where (a) 0.00, (b) 0.02, (c) 0.04, (d) 0.06 and (e) 0.08 sintered at 1150°C holding time 3hours	53
Figure 4.6	Hysteresis loops of $\text{Cu}_{0.15}\text{Zn}_{0.85}\text{La}_x\text{Fe}_{2-x}\text{O}_4$, [Where $x = 0.00, 0.02, 0.04, 0.06$ and 0.08] ferrites at room temperature 300K	55
Figure 4.7	Frequency dependent initial permeability of $\text{Cu}_{0.15}\text{Zn}_{0.85}\text{La}_x\text{Fe}_{2-x}\text{O}_4$, [where $x=0.00, 0.02, 0.04, 0.06$ and 0.08] ferrites sintered at 1150°C for holding time 3 hours	58
Figure 4.8	Frequency dependent imaginary permeability of $\text{Cu}_{0.15}\text{Zn}_{0.85}\text{La}_x\text{Fe}_{2-x}\text{O}_4$, [Where $x=0.00, 0.02, 0.04, 0.06$ and 0.08] ferrites sintered at 1150°C for 3 hours holding time	59
Figure 4.9	Frequency dependent loss factor of $\text{Cu}_{0.15}\text{Zn}_{0.85}\text{La}_x\text{Fe}_{2-x}\text{O}_4$, [Where $x=0.00, 0.02, 0.04, 0.06$ and 0.08] ferrites sintered at 1150°C for 3 hours	61
Figure 4.10	Frequency dependent real part of dielectric constant of $\text{Cu}_{0.15}\text{Zn}_{0.85}\text{La}_x\text{Fe}_{2-x}\text{O}_4$, [Where $x=0.00, 0.02, 0.04, 0.06$ and 0.08] ferrites sintered at 1150°C for holding time 3 hours	62
Figure 4.11	Frequency dependent imaginary part of dielectric constant of $\text{Cu}_{0.15}\text{Zn}_{0.85}\text{La}_x\text{Fe}_{2-x}\text{O}_4$, [Where $x=0.00, 0.02, 0.04, 0.06$ and 0.08] ferrites sintered at 1150°C for 3 hours	63
Figure 4.12	Variation of DC resistivity with La content (x) in $\text{Cu}_{0.15}\text{Zn}_{0.85}\text{La}_x\text{Fe}_{2-x}\text{O}_4$, [Where $x=0.00, 0.02, 0.04, 0.06$ and 0.08]	64

	ferrites sintered at 1150°C for 3 hours	
Figure 4.13	Temperature dependence DC resistivity of $\text{Cu}_{0.15}\text{Zn}_{0.85}\text{La}_x\text{Fe}_{2-x}\text{O}_4$, [where $x=0.00, 0.02, 0.04, 0.06$ and 0.08] ferrites sintered at 1150°C for holding time 3 hours	65

List of Tables

Table No.	Descriptions	Page no.
Table 3.1	Atomic /molecular mass of raw materials	26
Table 3.2	Calculation of total mass of the composition	27
Table 3.3	Calculation for 20 g sample preparation	27
Table 3.4	Various Shape and size of $\text{Cu}_{0.15}\text{Zn}_{0.85}\text{La}_x\text{Fe}_{2-x}\text{O}_4$ sample	30
Table 3.5	AC Measurement parameters	42
Table 4.1	Position of the X-ray peaks and corresponding miller indices for, $\text{Cu}_{0.15}\text{Zn}_{0.85}\text{La}_x\text{Fe}_{2-x}\text{O}_4$ [where $x = 0.00, 0.02, 0.04, 0.06$ and 0.08] ferrites	48
Table 4.2	Data of the lattice parameter (a), X-ray density (ρ_x), bulk density (ρ_B), porosity (P%) of $\text{Cu}_{0.15}\text{Zn}_{0.85}\text{La}_x\text{Fe}_{2-x}\text{O}_4$, [Where $x=0.00, 0.02, 0.04, 0.06$ and 0.08] ferrites sintered at 1150°C for 3 hours	52
Table 4.3	Average grain size for $\text{Cu}_{0.15}\text{Zn}_{0.85}\text{La}_x\text{Fe}_{2-x}\text{O}_4$ ferrites	54
Table 4.4	Saturation magnetization (M_s), coercivity (H_c) and remanent magnetization (M_r) of $\text{Cu}_{0.15}\text{Zn}_{0.85}\text{La}_x\text{Fe}_{2-x}\text{O}_4$, [where $x = 0.00, 0.02, 0.04, 0.06$, and 0.08] ferrites sintered at 1150°C holding time 3hours	56
Table 4.5	Values of initial permeability at different frequency range for $\text{Cu}_{0.15}\text{Zn}_{0.85}\text{La}_x\text{Fe}_{2-x}\text{O}_4$, [Where $x=0.00, 0.02, 0.04, 0.06$ and 0.08] ferrites	58

List of Symbols

XRD	=	X-Ray Diffraction
VSM	=	Vibrating Sample Magnetometer
SEM	=	Scanning Electron Microscopy
DC	=	Direct Current
RE	=	Rare Earth
FCC	=	Face Centered Cubic
T_N	=	Nell Temperature
ρ_B	=	Bulk density
ρ_x	=	X-ray density
ρ_{DC}	=	DC Resistivity
M_S	=	Saturation magnetization
M_r	=	Remanent magnetization
K_u	=	Anisotropy constant
H_c	=	Coercive force
μ_B	=	Magnetic moment in Bohr magneton.
μ	=	Permeability
μ'	=	Real part of the complex permeability
μ''	=	imaginary part of the complex permeability
ϵ	=	Dielectric constant
ϵ'	=	Real part of the dielectric constant
ϵ''	=	imaginary part of the complex permeability
D	=	Grain size
Φ	=	Magnetic Flux
I	=	Intensity of Magnetization
B	=	Magnetic induction
H	=	Magnetic field
a	=	Lattice parameter
$\tan \delta$	=	loss factor or loss tangent
λ	=	Wave length of the X-ray
[hkl]	=	Miller Indices of a peak
δ	=	Phase Angle

R	=	Resistance
T	=	Torque
B	=	External Magnetic Field
I	=	Intensity of Magnetization
χ	=	Magnetic Susceptibility
C	=	Capacitance of a Capacitor
C_0	=	Capacitance of a Capacitor with Vacuum
$F(\theta)$	=	Nelson Riley Function
Q	=	Quality Factor
RQF	=	Relative Quality Factor

CHAPTER I

INTRODUCTION

INTRODUCTION

1.1 Introduction

Ferrites are of ferromagnetic oxide materials with spinel structure having structural, magnetic and transport properties. Ferrimagnetism in ferrite is largely governed by Fe-Fe interaction as like the spin coupling of the 3d electrons. If the small amount addition of rare earth ions enters the spinel lattice, the RE-Fe interactions also appears 4f-3d coupling, which can lead to changes magnetic and transport properties. There has been a growing interest in soft ferrites due to their wide range of applications in magnetic recording media, electromagnetic data storage, sensors, and switches as well as in microwave devices, isolators, circulators, phase shifters for a several decades. The possibility of mixing metals in different compositions makes ferrites very eye-catching. The magnetic moments, the Neel temperature, the degree of the inversion and the super exchange strengths are some of the features that can be altered by introducing different metals into the ferrites [Horvath, 2000]. Different substitutions into soft ferrites have been incorporated to get electrical and magnetic properties [Ajmal and Maqsood, 2008]. The most important advances were made in ferromagnetism in the field of magnetic oxide. The advancement of high frequency ferrites was initiated by the work done by Snoek [Snoek, 1984] who found that associated with excellent properties in the high frequency range Cu-Zn, Mn-Zn and Ni-Zn ferrites provide a family of magnetic materials useful for radio and TV sets as carrier telephony as cores of inductors transformer and so forth.

Ferromagnetic interactions direct cation-cation is negligible because cations are separated by oxygen. When cations are bonded covalently to the oxygen ion, p-orbital of oxygen interact with d-orbital cations with anti-parallel spins of cations. This mechanism of indirect interaction is super-exchange. The magnetic properties of the ferrites are changeable. These can be modified by distribution of cations in 'A' and 'B' sites through substitution or doping. There are three types of interactions like A-O-B, B-O-B and A-O-A. Among them A-O-B interaction is the strongest one. Ni-Cu ferrite is inverse spinel where, half of the Fe^{3+} are in 'A' sites; remaining half and Ni, Cu share 'B' sites. When Cu is substituted for Zn, Cu preferentially enters into the 'B' sites by displacing a proportionate number of Fe^{3+} from 'B' to 'A' sites with a cation distribution. The most popular combinations are Ni-Zn [Ahmed *et al.*, 2004], Ni-Cu-Zn [Khan *et al.*, 2013], Mg-Zn [Hakim *et al.*, 2000] and Mg-Cu-Zn ferrites [Manjurul Huq *et al.*, 2008]. The magnetic

and electric properties of ferrite materials strongly depend on their chemical compositions and additives substitutions. A small amount of foreign ions in the ferrite can dramatically change the properties of ferrites. The magnetic properties of Zn-substituted ferrites have attracted considerable attention because of the importance of these materials for high frequency applications.

Zinc ferrite (ZnFe_2O_4) possesses a normal spinel structure, i.e., $(\text{Zn}^{2+})\text{A}(\text{Fe}_2^{3+})\text{BO}_4^{2-}$; where all Zn^{2+} ions reside on A sites and Fe^{3+} ions on B sites. Therefore, substitution of Cu by Zn in $\text{Cu}_{1-x}\text{Zn}_x\text{Fe}_2\text{O}_4$ is expected to modify the magnetic properties. However, no detail works have been found in the literature regarding structural and hysteresis behavior of mixed Cu-Zn ferrite. In this paper, we study the structural and hysteresis parameters of Cu-Zn ferrites. The electrical conduction and dielectric behavior of ferrites markedly depend on the preparation conditions such as sintering temperature, chemical composition, the quantity and type of additives. Dispersion in ac electrical resistivity, dielectric constant and loss tangent with frequency in polycrystalline ferrites is strongly dependent on the polarization process [Patil *et al.*, 1991] and is also related to the Verway conduction mechanism. At present, Bangladesh is totally dependent upon the imported ferrite cores and other soft magnetic materials. If we will develop rare earth doped ferrites in our country that may alleviate present problems of our country. Even though, improvements and innovation continue to take place; many new applications, theories and preparation technologies are currently under development in the field of ferrites.

In the present work, attempt will be made systematically to investigate the structural and magnetic properties of rare earth La^{3+} substituted Cu-Zn ferrites and it has been prepared by Standard Ceramic Method. The slight replacement of Fe by rare earth metal La by rare-earth metal La will reduce the sintering temperature which may affect to obtain homogeneous microstructure and enhance electromagnetic properties. It is ferromagnetic in nature and posses a cubic structure and can be used in various electromagnetic devices due to their high resistivity and high frequency tolerance. Finally, we used powder particles as starting materials whose uniform microstructure exhibiting better magnetic and electrical transport properties. The systematic research is still necessary for a more comprehensive understanding and properties of La doped Cu-Zn ferrite material system permeability application in high frequency range and magnetic properties are improved. In this research in soft magnetic materials and in rare earth metal doped ferrites, Bangladesh may develop a profitable electronic industry.

1.2 The Aims and Objectives of the Recent Work

This main objective has been the search for the best suited composition and preparation parameters for optimum performance of ferrite samples in respect of frequency response permeability and dielectrics. Ferrites are especially convenient for high frequency uses because of their high resistivity such as 10^2 to 10^{10} Ω -cm which higher than that of Fe. The high frequency response of the complex permeability is therefore very in determining the convenient frequency range in which a particular ferrite material can be used. The mechanism of eddy current losses and damping of domain wall motion can be understood from the relative magnitudes of the real and imaginary part of the complex permeability.

The rare earth substituted different ferrites are becoming the promising materials applications. Addition of small amount of rare earth ions to Cu-Zn ferrites samples produces a change in their magnetic and electrical as well as structural properties depending upon and amount of rare elements like La used. The main purpose of this work is to amalgamate La ions (La^{3+}) doped Cu-Zn ferrites, hence to study the effect of substitution of rare earth on the surface morphology, saturation magnetization, complex permeability, quality factors, transport properties like dielectric and electrical resistivity.

The main objectives of the present research are as follows:

- ❖ Preparation of various $\text{Cu}_{0.15}\text{Zn}_{0.85}\text{La}_x\text{Fe}_{2-x}\text{O}_4$ where $[x = 0.00, 0.02, 0.04, 0.06$ and $0.08]$ samples by solid state reaction technique.
- ❖ Determination of crystal structure density and porosity of the samples.
- ❖ Investigation of surface morphology, microstructure and compositional analyses using Scanning Electron Microscopy (SEM).
- ❖ Study of complex initial permeability as a function of frequency (100Hz - 120MHz) using Wayne Kerr Impedance Analyzer.
- ❖ Investigation of specific magnetization process using Vibrating Sample Magnetometer (VSM).
- ❖ Measurement of complex dielectric constant of various compositions over arrange of frequency (20Hz-120MHz)
- ❖ Measurement of resistivity using Electrometer Cathley.
- ❖ Optimization the concentration of La doped Cu-Zn ferrite for the best magnetic and transport properties.

1.3 Experimental Reason for This Research Work

$\text{Cu}_{0.15}\text{Zn}_{0.85}\text{La}_x\text{Fe}_{2-x}\text{O}_4$ [$x = 0.00, 0.02, 0.04, 0.06$ and 0.08] samples has been prepared by standard solid state reaction technique. High purity powders of CuO (99.9%), ZnO (99.9%), La_2O_3 (99.9%), Fe_2O_3 (99.9%) will be mixed thoroughly in an appropriate amount mixing will be performed in both dry and acetone. The mixed powders will be calcined at high temperature. After calcinations toroid and disk shaped sample will be prepared and will be sintered at various temperatures. The experimental methods that have been used in this work are as follows:

- ❖ Sintering of the samples has been carried out in a microprocessor controlled high temperature furnace department of Physics, Khulna University of Engineering & Technology (KUET), Khulna.
- ❖ The prepared sample would be characterized in terms of their crystal structure, unit cell parameters and phase presents in the prepared sample with the help of X-ray diffractometer (XRD) in the material science division, Bangladesh Atomic Energy Center (BAEC), Dhaka.
- ❖ Surface morphology of the samples has been investigated using SEM in the material science division, Bangladesh Atomic Energy Center (BAEC), Dhaka.
- ❖ Permeability, magnetic loss factor and quality factor as function of frequency have been determining using impedance analyzer in the department of Physics, Khulna University of Engineering & Technology (KUET), Khulna.
- ❖ Magnetizations of the samples have been measured as a function of field using VSM in the material science division, Bangladesh Atomic Energy Center (BAEC), Dhaka.
- ❖ AC electrical resistivity as a function temperature has been studied with the help of electrometer in the department of Physics, Khulna University of Engineering & Technology (KUET), Khulna.
- ❖ Dielectric properties as a function of frequency have been studied with the help of inductance meter department of Physics, Khulna University of Engineering & Technology (KUET), Khulna.

Finally, the structural properties of Fe replaced La in Cu-Zn ferrites such as grain size, lattice parameters is modified due to the incorporation La^{3+} ions. The saturation magnetization, the quality factor, electrical resistivity of Cu-Zn ferrites is also expected to

improve and accumulated results have been interpreted on the basis of existing theories of magnetism.

1.4 Importance of Ferrites

Ferrites are primarily used as inductive components in a large variety of electronic circuits such as low noise amplifiers, filters, voltage controlled oscillators, impedance matching networks for instance. The basic components to produce the inductance are very soft ferrite and a metallic coil. Multilayer chip inductors for high frequency circuit's applications use sheets made of dielectric ceramics instead of ferrite industry. Rare earth ferrites are used widely now-a-days due to their following applications:

- ❖ Ferrites are part of low power and high flux transformers which are used in television.
- ❖ Small antennas are made by winding a coil on ferrite rod used in transistor radio receiver
- ❖ In computer, non volatile memories are made of ferrite materials. They store information even if power supply fails. Non-volatile memories are made up of ferrite materials as they are highly stable against severe shock and vibrations.
- ❖ Ferrites are used in microwave devices like circulators, isolators, switch phase shifters and in radar circuits.
- ❖ Ferrites are used in high frequency transformer core and computer memories i.e. computer hard disk, floppy disks, credit cards, audio cassettes, video cassettes and recorder heads.
- ❖ Ferrites are used to produce low frequency ultrasonic waves by magnetostriction.
- ❖ Nickel alloys are used in high frequency equipments like high speed relays, wideband transformers and inductors. They are used to manufacture transformers, inductors, small motors, synchros and relays. They are used for precision voltage and current transformers and inductive potentiometers.
- ❖ They are used as electromagnetic wave absorbers at low dielectric values.
- ❖ Ferrites are important components for the latest products, such as cellular phones, video cameras, note book computers, hard temperatures and floppy drives.
- ❖ Ferrites for the applications in producing multilayer-type chips mainly because these oxide.

1.5 Review of the Earlier Research Work

Remarkable properties such as high permeability, high quality factor, high stability of initial permeability with temperature and time, high resistivity, controlled coercive force etc. have appositely placed Cu-Zn ferrites as high demandable materials to both researchers and manufacturers. The effect of compositional variation on magnetic susceptibility, saturation magnetization (M_s), Curie temperature (T_c), magnetic moment, structural properties and transport property of $Cu_{1-x}Zn_xFe_2O_4$ ferrites have been studied by Rana *et al.*, [1998]. The T_c and M_s increases from Zn content 0 to 0.75. From these ferrites Y-K angles of Zn substituted ferrites, it was concluded that the mixed Zn-ferrites exhibit a non-coinearity of the Y-K type while $CuFe_2O_4$ shows a Neel type of ordering.

Shahida Akhter *et al.*, [2011] were synthesized $Cu_{1-x}Zn_xFe_2O_4$ ferrite with $x = 0.5$ using the standard solid state reaction technique. T_c has been determined from the temperature dependence of permeability and found to decrease with increasing Zn content. The anomaly observed in the temperature dependence of permeability was attributed to the existence of two structural phases: cubic phase and tetragonal phase. Low field hysteresis measurements have been performed using a B-H loop trace from which hysteresis parameters have been determined.

Abbas *et al.*, [1995] were done by the solid state technique $Cu_{1-x}Zn_xFe_2O_4$ ferrite with $x = 0.1, 0.2$ and 0.3 studying of sintering effect on structural and electrical properties. Sintering temperature has a pronounced effect on density and grain size in which density decreased and grain size increased with increasing of sintering temperature. The Cu-Zn mixed ferrites viz. were synthesized by Dawoud and Shaat, [2006]. Microstructure and compositional features were studied by scanning electron microscope and energy dispersive XRD analysis. Magnetic properties were measured by B-H hysteresis loop tracer technique. The variation of M_s , remnant magnetization and coercivity were studied as a function of Zn content. The substitution of Zn ions plays decisive role in changing structural and magnetic properties.

Hossain *et al.*, [1917] reported the impact Y^{3+} substituted Ni-Zn ferrites show additional peaks other than spinel structure and corresponding to a second orthoferrite phase. The increase in density and grain growth of the samples may be attributed to the liquid phase at constant sintering temperature. Y^{3+} doped Ni-Zn ferrites are biphasic homogeneous microstructure constituted of dark ferrite matrix grains and small whitish grain at the grain junction. The grain boundaries of the lower conductivity were found to

be ferrite at lower frequencies while ferrite grains of high conductivity are effective at high frequency.

Roy and Bena, [2008] reported the impact of Sm^{3+} substitution showed improved resistivity Ni-Cu-Zn ferrites. They also discussed relative density and grain size of ferrites increased with increase Sm^{3+} substitution. Increased densification may be due to the appearance of excess Ni, Zn and Cu composed with Fe in the composition.

Sattar and El-Shokrofy, [1997] investigated Cu-Zn ferrites doped with rare earth ions like La, Sm, Nd, Gd and Dy. They found that all samples were of high relative density and low porosity. The magnetization of the samples with Sm and La were higher than that of the undoped ones. The magnetization values of the sample with Nd may be higher or lower than that of the undoped ones depending on the applied magnetic field. The samples with La, Sm and Nd had higher values of relative permeability (μ_r) than that of undoped samples while those with Gd and Dy had lower values μ_r than that of undoped ones.

Khan *et al.*, [2013] reported that Ni-Cu-Zn ferrites are well established soft magnetic materials for MLCI application because of their relatively low sintering temperature, high permeability in the rf-frequency region and high electrical resistivity and studied complex permeability spectra of Ni-Cu-Zn ferrites. The particle size increase with increasing the sintering temperature and it was also found that the real part of initial permeability of the low frequency region decreases.

Hossain *et al.*, [2015] introducing optimally Eu^{3+} substituted Ni-Zn ferrites is possible to develop good magnetic materials. Eu^{3+} ions replace the metallic cations in tetrahedral A-sites or octahedral B-sites to improve various properties of the samples. Introducing a very poor amount of rare earth ions may significantly changes the microstructure, electrical, magnetic as well as optical properties of the ferrites composites.

Shahida Akter *et al.*, [2011] analysed a series of $\text{Cu}_{1-x}\text{Zn}_x\text{Fe}_x\text{O}_4$. They found that the presence of Zn ions causes appreciable changes in the structure. They observed that the XRD patterns and confirm the samples were well crystallized and single phase. The lattice constant was found to increase linearly with increasing Zn content in the Cu-Zn ferrite.

1.6 Outline of the Thesis

The thesis has been configured into five chapters which are as follows:

Chapter I: Introduction

In this chapter, presents a brief introduction to Cu-Zn ferrites and organization of thesis. This chapter incorporates background information to assist in understanding the aims and objectives of this investigation, and also reviews recent reports by other investigators with which these results can compared.

Chapter II: Theoretical Background

In this chapter, a briefly describe theories necessary to understand magnetic materials as well as ferrites, classification of ferrites, cation distribution, super exchange interaction, two sub lattices modules etc. have been discussed in details.

Chapter III: Experimental Background

In this chapter, the experiment procedures are briefly explained along with description of the sample preparation, raw materials. This chapter deals with mainly the design and construction of experimental and preparation of ferrite samples. The fundamentals and working principles of measurement set up are discussed.

Chapter IV: Results and Discussion

In this chapter, results and discussion are thoroughly explained. The various experimental and theoretical studies namely Effect of La Substitution on the Structural, Electrical and Magnetic properties of Cu-Zn Ferrites are presented and discussed step by step.

Chapter V: Conclusion

In this chapter, the results obtained in this study are summarized. Suggestions for future works on these studies are included.

Finally, a complete list of references and publications as been given towards the end of this chapter.

CHAPTER II

THEORETICAL BACKGROUND

THEORETICAL BACKGROUND

2.1 Overview of Rare Earth Ferrites

The rare earth substituted different ferrites are becoming the promising material for different applications. Addition of small amount of rare earth ions to ferrite samples producing a change in their magnetic and electrical as well as structural properties depending upon the types and the amount of rare earth elements used. Many researches have been carried out on the influence of different rare earth atoms like La, Sm, Gd, Nd, Dy, Tb, Ce, Th, Y, Eu etc on the properties of ferrites. The results of these researches show how that different rare earth atoms behave differently in spinel ferrite. Rare earth metals are actually not as rare as their name might imply. They are simply more difficult to mine than most metals and generally don't accumulate into rich ores. This rarity, combined with the demand for the metals in high-tech applications, brings about economic and political complications that make some of the most interesting metals even more exciting. The rare earth elements are all metals, and the group is often referred to as the "rare earth metals". These metals have many similar properties and that often causes them to be found together in geologic deposits. They are also referred to as "rare earth oxides" because many of them are typically sold as oxide compounds. Rare earth elements are not as "rare" as their name implies. Thulium and lutetium are the two least abundant rare earth elements - but they each have an average crustal abundance that is nearly 200 times greater than the crustal abundance of gold [Rare Earth Elements]. However, these metals are very difficult to mine because it is unusual to find them in concentrations high enough for economical extraction.

Rare earth ions (RE) can be divided into two categories: one with the radius closes to Fe ions and other with ionic radius larger than Fe ions. The difference in their ionic radii will lead to micro strains, which may cause domain wall motion resulting in deformation of the spinel structure. The RE ions commonly reside at the octahedral sites by replacing Fe^{3+} ions and have limited solubility in the spinel lattice due their large ionic radii. The better properties of ferrites can be achieved through proper doping of rare earth metals and recently RE doped ferrites become interesting due to their superiority for various applications such as structural, magnetic and electrical properties over other doped ferrite systems [Bharathi *et al.* 2009, Peng *et al.* 2011, Guo *et al.* 2010 and Nikumbh *et al.* 2014].

Doping the parent spinel ferrite with RE ions leads to structural disorder and lattice strain, thereby increasing the electrical and magnetic parameters [Jacobo *et al.* 2004]. The difference in their ionic radii will lead to micro strains, which may cause domain wall motion resulting in deformation of the spinel structure. The RE ions have unpaired 4f electrons and the strong spin orbit coupling of the angular momentum. Moreover, 4f shell of RE ions is shielded by $5S^25P^6$ and almost not affected by the potential field of surrounding ions. Doping RE ions into spinel type ferrites, the occurrence of 4f-3d couplings which determine the magneto-crystalline anisotropy in spinel ferrite can also improve the electric and magnetic properties of spinel ferrites [Jing *et al.* 2006, Jing *et al.* 2007, Vanuitert 1955 and Kolekar *et al.* 1995]. Spinel ferrites ceramic are widely used in microwave devices to control transmission path, frequency, amplitude and phase of microwave signals. Accurate dielectric and magnetic properties measurement at the operational frequency and temperature ranges are needed for optimized development of these devices, as well as to assist in the manufacture of the ferrite [Jie *et al.* 2010]. The structured magnetic materials have an interesting area of study because of its possible applications in a variety of widely areas ranging from information technology to biotechnology [Bahadur *et al.* 2005]. The properties of ferrites are being improved due to the increasing trends in ferrite technology. It is believed that there is a bright future for ferrite technology. Ferric magnetism in ferrite is largely governed by Fe-Fe interaction, i.e. the spin coupling of the 3d electron. In view of the great interest of RE doped Cu-Zn ferrites, both their technological applications and theoretical understanding of the mechanisms involved, the present work is aimed at finding the effect La ions. A large number of workers are engaged in research to bring about improvement on the qualities of RE doped Cu-Zn ferrites has been improve in all aspects than the mother alloy Cu-Zn ferrites.

2.2 Ferrites

Ferrites are extensively studied materials because of their interesting physical, structural and magnetic properties. Ferrites is fabricated into commercially useful magnetic material during by Snoek, 1933. Now a day's many researchers are trying to enhance the magnetic properties. Ferrites are electrically non-conductive ferrimagnetic ceramic compound materials, consisting of various mixtures of iron oxides such as Hematite (Fe_2O_3) or Magnetite (Fe_3O_4) and the oxides of other metals like NiO, CuO, ZnO, MnO, CoO. They are both electrically nonconductive and ferrimagnetic, meaning

they can be magnetized or attracted to a magnet. On the other hand ferrites are a class of ferrimagnetic ceramic chemical compounds consisting of mixtures of various metal oxides, usually including iron oxides. Their general chemical formula may be written as AB_2O_4 , where A and B represent different metal cations. These ceramic materials are used in applications ranging from magnetic components in microelectronics.

Very high permeability is restricted to certain temperature ranges and the shapes of permeability versus temperature curves are strongly affected by any inhomogeneity in the ferrite structure [Roess 1971]. High permeability is affected by the microstructure of the ferrites. At high frequencies ferrites are considered superior to other magnetic materials because they have low eddy current losses and high DC electrical resistivity. The DC electrical resistivity of ferrites at room temperature can vary deep-ending upon the chemical composition. The sintering process plays a dominant role in many magnetic properties of ferrites.

2.2.1 Types of ferrites

Ferrites are complex magnetic oxides that contain the Fe_2O_3 and their basic magnetic component. They are both electrically nonconductive and ferromagnetic, means that magnetized or attractive to a magnet. The crystallography of ferrites fall in a natural manner into three types: (i) the cubic ferrites of spinel type, (ii) The cubic ferrites of the garnet type and (iii) the hexagonal ferrites. The magnetic ferrites fall into two groups of different crystal structures as shown below:

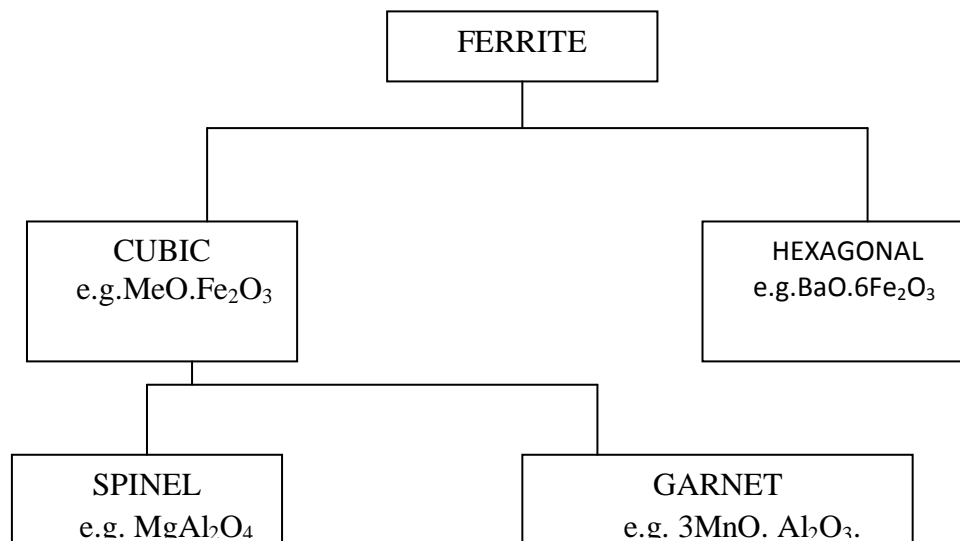


Figure 2.1: Classification of Ferrites

Ferrites are classified into two categories based on their coercive field strength.

They are:

- (i) Soft ferrite with coercive field strength $< 100\text{Oe}$
- (ii) Hard ferrite with coercive field strength $> 1250\text{Oe}$.

2.2.2 Spinel Ferrites

They are also called cubic ferrite. Spinel is the most widely used family of ferrite. High values of electrical resistivity and low eddy current losses make them ideal for their use at microwave frequencies. The spinel structure of ferrite as possessed by mineral spinel MgAl_2O_4 was first determined by Bragg and Nishikawa in 1915. The chemical composition of a spinel ferrite can be written in general as MeFe_2O_4 , where Me is a divalent metal ion such as Co^{2+} , Zn^{2+} , Fe^{2+} , Mg^{2+} , Ni^{2+} , Cd^{2+} , Cu^{2+} or a combination of these ions.

The unit cell of spinel ferrite is fcc with eight formula units per unit cell. The formula can be written as $\text{M}_8\text{Fe}_{16}\text{O}_{32}$. The anions are the greatest and they form an fcc lattice. Within these lattices two types of interstitial positions occur and these are occupied by the metallic cations. There are 96 interstitial sites in the unit cell, 64 tetrahedral (A) and 32 octahedral (B) sites. The sites are so narrow because they are surrounded by four and six ions at equal distances respectively shown in Figure 2.2.

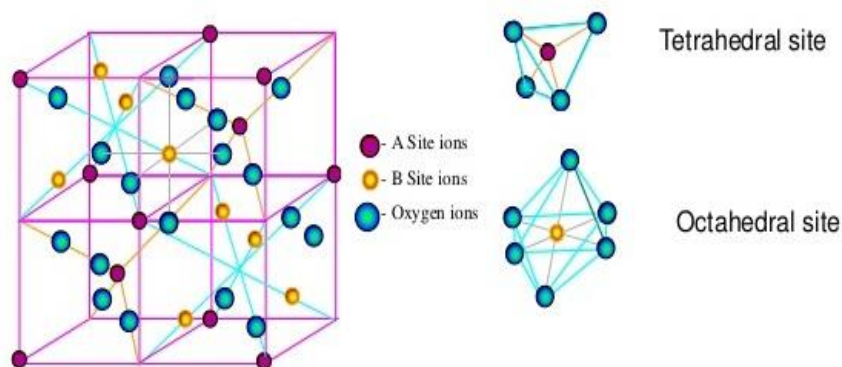


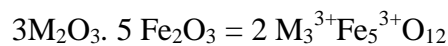
Figure 2.2: Crystal Structure of spinel ferrite

The lattice characteristics of a spinel includes a face centre cubic (fcc) site for two oxygen atoms and two cationic sites occupying A and B sites [Virginia Fuentes *et. al.* 1987 and Anderson 1963] in a spinel, there are 64 A sites, 32 B sites and 32 oxygen sites in a unit

cell. Due to their exchange coupling, spinel ferrites are ferrimagnetically aligned where all of the moment of A sites are aligned parallel with respect to one another while moments of A and B sites are anti parallel to each other. The charge neutrality requires the presence of the cations within the structure to counter balance the charge of these oxygen anions. These cations rest on two types of interstitial sites to preserve the charge neutrality namely A and B sites. The magnetic properties of spinel ferrites are generally influenced by composition and cation distributions. Variation of cation distribution between the cationic sites lead to different electrical and magnetic properties even if the composition of cations over A and B sites is determined by their ionic radius, electronic configuration and electrostatic energy in the spinel lattice.

2.2.3 Cubic Ferrites Garnets

The mineral garnet refers to group of mixed oxides, of which the widely known one has the chemical formula $Mn_3Al_2Si_13O_{12}$, or equivalently $3MnO \cdot Al_2O_3 \cdot 3Si_2O_3$ single magnetic garnets have the general formula.



It is to be noted that in magnetic garnets the 24 positive charge units per formula units are divided unequally between the ferrite ions (15 units) and another species of trivalent ions (9 units). Technically metal garnets are those with $M = Sm, Eu, Gd, Tb, Dy, Ho, Er, Tm, Yb$ and Yttrium. They are known as rare garnets and one of the cubic garnet structures shown in Figure 2.3. A code system has been adopted to name them. REG stands for the rare –earth garnets, GDIG for gadolinium-iron garnet ($Gd_3 Fe_5O_{12}$) etc. Garnets crystallize in the cubic system with two fifths of the ferrite ions forming a bcc lattice, like ferros spinels, the garnets too. Pack a large number (160) of ions in eight unit's formula unit cell.

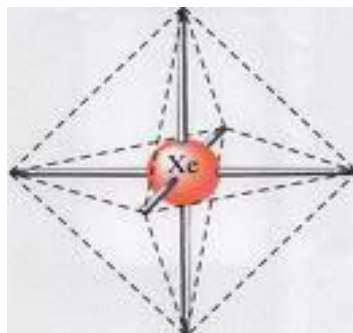


Figure 2.3: Cubic ferrite of garnet

The lattice constant is nearly 12.5^0A about 50% larger than those ferrosinzel. Also the crystal structure of garnets is more complicated than the spinel structure because of the size ($0.85\text{-}1.10^0\text{ A}$) of the M^{3+} ions. They are too large to be accommodated at the interstitial sites between the oxygen ions. Hence the oxygen ions are prohibited from forming a close packed structure as in the spinel. The general formulas for the unit cell of a pure iron garnet have eight formula units of $\text{M}_3\text{Fe}_5\text{O}_{12}$, where M is trivalent rare earth ions (Y, Gd, Dy). Their cell shape is cubic and the edge length is about 12.5^0A . They have complex crystal structures. They are important due to their application in memory structure [Neel 1948].

2.2.4 Ortho-ferrites

Ortho-ferrites have the general formula MFeO_3 , where, M is a large trivalent metal ion, such as rare-earth ion or Y. They crystallize in a distorted perovskite structure with an orthorhombic unit cell. These ortho-ferrites show a weak ferromagnetism, which has been attributed to the small canting in the alignment of two anti-ferromagnetically coupled lattices. The canting angle is of the order of 10^{-2} radian but is sufficient to introduce a small net ferromagnetic moment perpendicular to the antiferromagnetic axis.

2.2.5 Hexagonal Ferrites

Hexa ferrites are hexagonal or rhombohedral ferromagnetic oxides with formula $\text{MFe}_{12}\text{O}_{19}$, where M is an element like Barium, Lead or Strontium and one of the crystal structure shown in Figure 2.4. The third type oxygen ferrites are often called the barium ferrites.

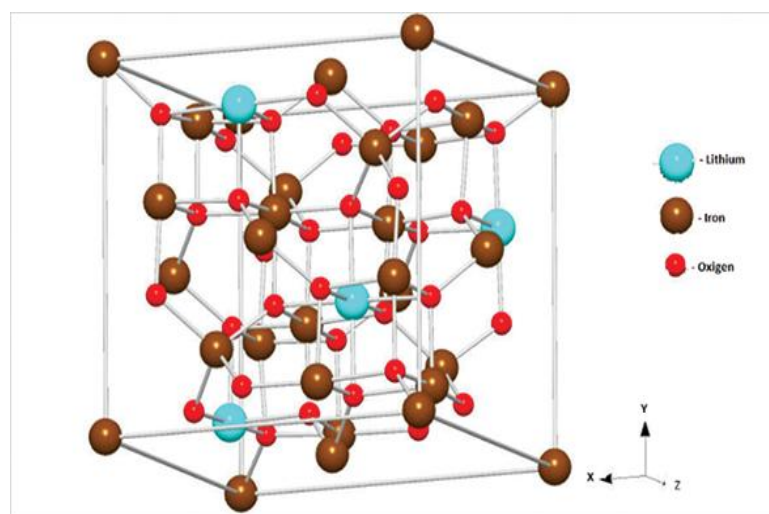


Figure 2.4: Crystal structure of hexagonal ferrite

These compound usually cation BaO, in addition to Fe₂O₃, as the basic component oxide. They are also known as magneto plumbites. The common chemical formula of barium ferrites is $1(\text{BaO}) \cdot m(\text{MO}) \cdot n(\text{Fe}_2\text{O}_3)_n$ or $\text{Ba}^{3+} \cdot \text{Mm}^{2+} \text{Fe}_{2n}^{3+} \text{O}_{1+m+3n}^{2-}$, where 1 is much more complex than the previous two in both in terms of composition of barium ferrites may be complex than the previous two in both in terms of composition of barium ferrites may be changed one is to vary the M³⁺ ions. Mg, Mn, Fe, Co, Ni, Cu and Zn are found suitable for the formation of hexagonal ferrites. Another way to alter the values of l, m and n. Basic compositions are found at 1-0-6(M), 1-2-8 (M₂W), 2-2-6 (M₂Y) and 3-2-12(M₂). In these ferrites, oxygen ions have closed packed hexagonal crystal structure. They are widely used as permanent magnets and have high coercivity. They are used at very high frequency. Their hexagonal ferrite lattices are similar to the spinel structure with closely packed oxygen ions, but there are also metal ions at some layers with the same ionic radii as that of oxygen ions. Hexagonal ferrites have larger ions than that of garnet ferrite and are formed by the replacement of oxygen ions. Most of these larger ions are barium, strontium or lead.

2.3 Types of Spinel Ferrites

The spinel ferrites have been classified into three categories due to the distribution of cations on tetrahedral (A) and Octahedral (B) sites.

- ❖ Normal spinel ferrites
- ❖ Inverse spinel ferrites
- ❖ Intermediate or Mixed spinel ferrites

2.3.1 Cation Distribution in Spinel

The cation distribution in the spinel $\text{M}^{2+}\text{M}^{3+}\text{O}_4$ can be as follows:

❖ Normal

The Me^{2+} cations are in tetrahedral positions, while the two M^{3+} cations are in octahedral sites. The square brackets are generally used to present the octahedral sites, i.e. $\text{M}^{2+}\text{M}^{3+}\text{O}_4$

❖ Inverse

In the case the M^{2+} cation and one of the M^{3+} cations are in octahedral positions while the second M^{3+} cation occupies a tetrahedral positions. The arrangement is as. $\text{M}^{3+} [\text{M}^{2+}\text{M}^{3+}]\text{O}_4$.

❖ Intermediate

The arrangement of the form like $M^{3+}_{1-\delta} M^{2+}_{\delta} [M^{3+}_{1-\delta} M^{2+}_{1+\delta}]O_4$ is often referred as intermediate, where δ is called the inversion parameter. $\delta = 0.0$ for completely normal and $\delta = 1.0$ for completely inverse spinels and $0 < \delta < 1$ for intermediate spinels [Verway and Heilmann 1947 and William 2003].

The factors affecting the cation distribution over A and B sites are as follows:

- ❖ The size of the cations
- ❖ The electronic configuration of cations
- ❖ The electronic energy
- ❖ The saturation magnetization of the lattice

Smaller cations (trivalent ions) prefer to occupy the A-sites. The cations have special preference for A and B sites and the preference depends on the following factors:

- ❖ Ionic radius
- ❖ Size of interstices
- ❖ Sintering temperature and
- ❖ Orbital preference for the specific coordination.

The preference of cations is according to Verway- Heilmann scheme

- ❖ Ions with strong preference for A-sites Zn^{2+} , Cd^{2+} , Ga^{2+} , In^{3+} , Ge^{4+} .
- ❖ Ions with strong preference for B-sites Ni^{2+} , Cr^{3+} , Ti^{4+} , Sn^{4+} .
- ❖ Indifferent ions are Mg^{2+} , Al^{3+} , Fe^{2+} , Co^{2+} , Mn^{2+} , Fe^{3+} , Cu^{2+} .

2.4 Soft Ferrites

At high frequency metallic soft magnetic materials simply cannot be used due to the eddy current losses. Therefore soft ferrites, which is ceramic insulators, becomes the most desirable material. These materials are ferrimagnetic with a cubic crystal structure and the general composition $MO.Fe_2O_3$ where M is a transition metal such as nickel, manganese, magnesium, zinc, cobalt or cadmium. The magnetically soft ferrites first came into commercial production in 1948 and shown in Figure 2.5(a).

Mn-Zn ferrite, sold commercially as ferroxcube, can be used at frequencies up to 10MHz, for example in telephone signal transmitters and receivers and in switch mode power supplies. For these type of application the driving force to increase frequency is to allow miniaturization. Additionally, parts of the family of soft ferrites are the microwave ferrites e.g. Yttrium iron garnet. These ferrite are used in the frequency range from 100 MHz to 500GHz. For waveguides, for electromagnetic radiation, and in microwave

device such as phase shifters. Application of soft ferrite include: cores for electro-magnets, electric motors, transformers, generators, and other electrical equipment.

2.5 Hard Ferrites

Hard ferrites are difficult to magnetized or demagnetized. Hard magnets are characterized by high remanent inductions and high coercivities are shown in Figure 2.5(b). The higher coercivity means the materials are very resistant to becoming demagnetized an essential characteristic for a permanent magnet. They also conduct magnetic flux well and have a high magnetic permeability. This enables these so-called ceramic magnets to store stronger magnetic fields than iron itself. They are cheap and are widely used in household products such as refrigerator magnets. They generally exhibit large hysteresis losses. Hard ferrite referred to as permanent magnets retain their magnetism after being magnetized. Hard ferrite likes Ba-ferrite, Sr-ferrite, Pb-ferrite are used in communication device operating with high frequency currents because of their high resistivity, negligible eddy currents and lower loss of energy due to Joule heating and hysteresis. These are found useful in many applications including fractional horse-power motors, automobiles, audio and video-recorders, earphones, computer peripherals, and clocks.

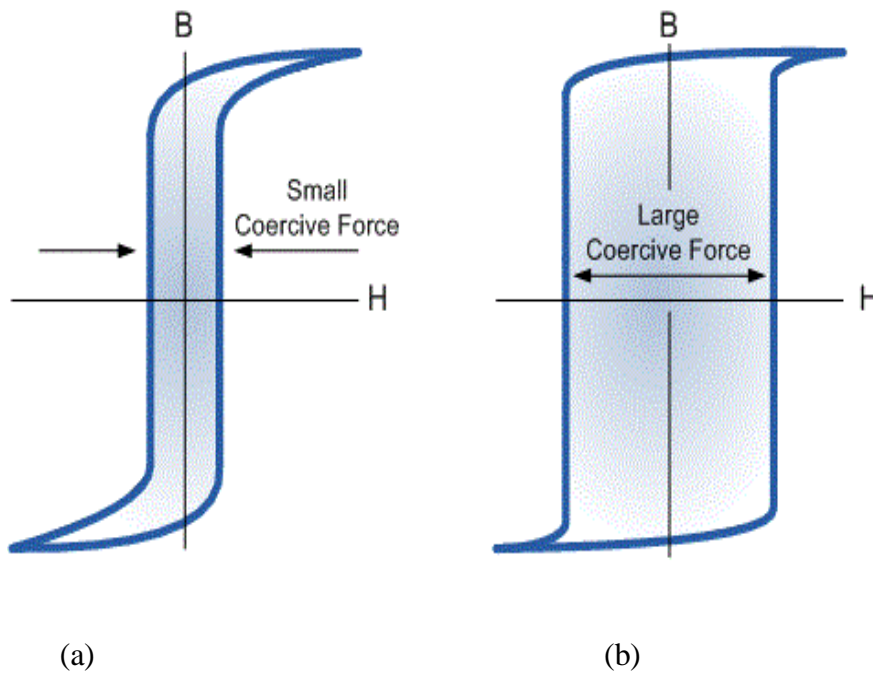


Figure 2.5: (a) Soft Ferrite, (b) Hard Ferrite

2.6 Magnetization Process

A review of the magnetization process, namely the response of ferro-(ferri) magnetic material (bulk) to an applied field with a semi-microscopic approach is presented. In ferro-or ferri-magnetic material, the magnetization curves, especially in low magnetic fields differ widely from sample to sample and as a function of the magnetic history of the sample i.e., of the previous fields which have been successively applied.

2.6.1 Magnetization Curve

For unmagnetized bulk materials, there is a zero net magnetic moment. It can be predicted that there will be an infinite number of degree of magnetization between the unmagnetized and saturation conditions, when the material is subjected to an external magnetic field. These extreme situations are corresponds respectively to random orientation of domains complete alignment is one direction with elimination of domain walls. If we start with a demagnetized specimen and increase the applied magnetic field, the bulk material will progressively magnetized by the domain dynamics. The magnetization of the sample will follow the course as shown in Figure 2.6 [Smit and Wijn 1959]. The slop from the origin to a point on the curve r the ratio $\frac{M}{H}$ is defined as magnetic susceptibility. This curve is called magnetization curve. This curve is generally perceived as being made of three major portions.

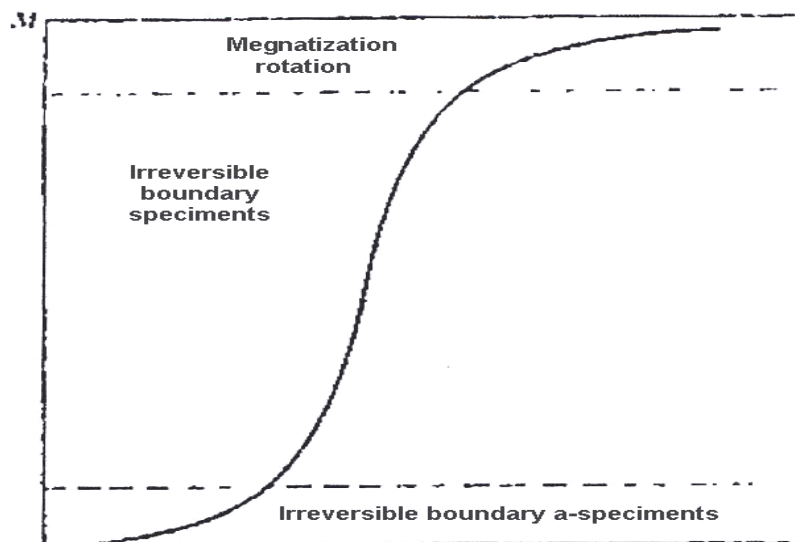


Figure 2.6: Domain dynamics during various parts of the magnetization curve

The first, the lower section, is the initial susceptibility region and characterized by reversible domain wall movements and rotations. By reversible means that after the magnetization slightly with an increase in field the origin magnetization can be reversed if the field is reduced to initial value. The condition of the displacement walls to an initial permeability is entirely dependent on the sort of material studied. In the second stage magnetization curve if the field is increased, the intensity of the magnetization increases more drastically is called the irreversible magnetization range. This range is obtained mainly by the reversible domain wall motion from one stable state to another.

If the field is increased further, the magnetization curve less step and its process become reversible once more. In the third section of magnetization curve, the displacement of domain walls have all ready been completed and the magnetizations take place by rotation magnetization. This range is called rotation magnetization range. Beyond this range the magnetization gradually approaches to saturation magnetization shown in Figure 2.6.

2.7 Theory of Initial Permeability

Permeability is namely defines as the proportional constant between the magnetic field induction B and applied intensity H:

$$B = \mu H \quad (2.1)$$

If a magnetic material is subjected to an AC magnetic field as given below:

$$H = H_0 e^{i\omega t} \quad (2.2)$$

Then it is observed that the magnetic flux density B experiences a delay. The delay is caused due to presence of various losses and is thus expressed as

$$B = B_0 e^{i(\omega t - \delta)} \quad (2.3)$$

where δ is the phase angle and marks the delay of B with respect to H. The permeability is then given by

$$\mu = \frac{B}{H} = \frac{B_0 e^{i(\omega t - \delta)}}{H_0 e^{i\omega t}} \quad (2.4)$$

$$= \frac{B_0 e^{-i\delta}}{H_0} = \mu' - i\mu'' \quad (2.5)$$

Where,

$$\mu' = \frac{B_0}{H_0} \cos \delta \quad (2.6)$$

$$\mu'' = \frac{B_0}{H_0} \sin \delta \quad (2.7)$$

The real Part μ' of complex permeability μ as expressed in equation (2.6) represent the component of B which is in phase with H, so it corresponds to the normal permeability. If there is no losses, we should have $\mu = \mu'$, The imaging part μ'' corresponds to the part of B which is delayed by phase angle arranging up to 90° from H. The presence of such a component requires a supply of energy to maintain the alternating magnetization regardless of the origin of delay.

The ratio of μ'' to μ' gives

$$\frac{\mu''}{\mu'} = \frac{\frac{B_0}{H_0} \sin \delta}{\frac{B_0}{H_0} \cos \delta} = \tan \delta \quad (2.8)$$

This $\tan \delta$ is called the loss Factor or loss tangent. The Q-Factor or quality factor is defined as the reciprocal of this loss factor, i.e

$$Q = \frac{1}{\tan \delta} \quad (2.9)$$

2.8 Dielectric Constant

Dielectric constant is defined as the ratio of the capacitance of a capacitor filled with a given dielectric to the capacitance of the same capacitor with vacuum. It is a number without dimensions, a quantity measuring the ability of a substance to store electrical energy in an electrical field. If C represents the capacitance of a capacitor with dielectric and C_0 represents the capacitance of the same capacitor with vacuum, then the dielectric constant (ϵ') can be given by

$$\epsilon' = \frac{C}{C_0} \quad (2.10)$$

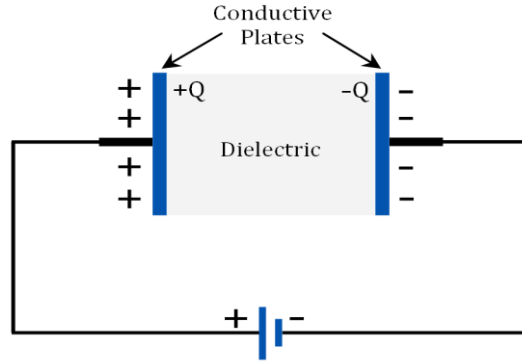


Figure 2.7: Schematic illustration of capacitive cell

But capacitance C of a parallel plate capacitor can be expressed as

$$C = \frac{\epsilon A}{d} \quad (2.11)$$

where, A is the area of each plate, d represents the separation between the plates and ϵ represents the permittivity of the dielectric material within the capacitor.

If ϵ_0 represents the permittivity of the free space, then from equation (2.10) we get

$$\epsilon' = \frac{\epsilon}{\epsilon_0} \quad (2.12)$$

Therefore, dielectric constant can also be defined as the ratio of the permittivity of a substance to the permittivity of free space. It is an expression of the extent to which a material concentrates electric flux, and is the electrical equivalent of relative magnetic permeability.

2.8.1 Dependence of Dielectric Constant on Frequency

Polarization systems respond to an electrical field by shifting their masses around and forms dipoles. These shifted masses are accelerated and de-accelerated with the change of the applied field which takes some time. Therefore, the polarization mechanism of a system depends on the frequency of the applied electrical field. Alternating electrical field induces alternating forces to the dipoles. Since the dipole response to a field involves the movement of masses, inertia will prevent the arbitrarily fast movements. When the frequency of the applied field increases, this movement of dipoles also increases. At high frequency, the dipoles are unable to cope with it. So at very high frequencies all movement of dipoles will 'die out' and there will be no response of the dipoles to the frequency field [Dai *et al.* 2012]. Dielectric constant (ϵ') is a measure of polarization of a system, it also depends on the frequency of the applied field. In general as frequency increases, its dielectric constant drops. But for some material the dielectric

constant can increase with the increase in frequency due to the parasitic effect but only at the low temperature.

2.9 DC Resistivity of Ferrites

Extensive investigation into the origin of the electrical conductivity of the spinels has been carried out by Verwey *et al.* 1947 and Jonker 1959. The resistivity of ferrites at room temperature can vary, depending on chemical composition between about 10^{-2} to higher than 10^{+11} ohm-cm. The low value of resistivity is due to the simultaneous presence of ferrous and ferric ions on equivalent lattice sites (octahedral). For example Fe_3O_4 at room temperature has resistivity of approximately 7×10^{-3} Ohm-cm and Fe_2O_4 with some deficiency in iron and sintered in a sufficiently oxidizing atmosphere so that the product contains no ferrous ions can have a resistivity higher than 7×10^6 ohm-cm. To make high resistivity ferrites one must sure that there are no ferrous ions in the stoichiometric ferrites.

Temperature dependent resistivity of ferrites follows Arrhenius relation [Smit and Wijn 1959]:

$$\rho = \rho_0 e^{\frac{E_a}{kT}}, \quad (2.13)$$

Where, ρ is the resistivity and E_a is the activation energy required for hopping of an electron from one lattice site to another.

2.10 Microstructure

A polycrystal is much more than many tiny crystals bonded together. The interfaces between the crystals, or the grain boundaries which separate and bond the grains, are complex and interactive interfaces. The whole set of a given material's properties of mechanical, chemical and especially electrical and magnetic depend strongly on the nature of the microstructure. The grain boundary is the region, which accommodates the difference in crystallographic orientation between the neighboring grains. For certain simple arrangements, the grain boundary is made of an array of dislocations whose number and spacing depends on the angular deviation between the grains. The ionic nature of ferrites leads to dislocation patterns considerably more complex than in metals, since electrostatic energy accounts for a significant fraction of

the total boundary energy. For low-loss ferrite, Goldman 1999 states that the grain boundaries influence properties by [Yan and Johnson 1978]

- (i) Creating a high resistivity intergranular layer.
- (ii) Acting as a sink for impurities which may act as a sintering aid and grain growth modifiers.
- (iii) Providing a path for oxygen diffusion, which may modify the oxidation state of cations near the boundaries.

In addition to grain boundaries, ceramic imperfections can impede domain wall motion and thus reduce the magnetic property. Among these are pores, cracks, inclusions, second phases, as well as residual strains. Imperfections also act as energy wells that pin the domain walls and require higher activation energy to detach. They affect the domain dynamics and are responsible for a much greater share of the degradation of properties than would expect grain growth kinetics depends strongly on the impurity content. A minor do pant can drastically change the nature and concentration of defects in the matrix, affecting grain boundary motion, pore mobility and pore removal [Yan and Johnson 1978]. The effect of a given do pant depends on its valence and solubility with respect to host material. If it is not soluble at the sintering temperature, the do pant becomes a second phase which usually segregates to the grain boundary.

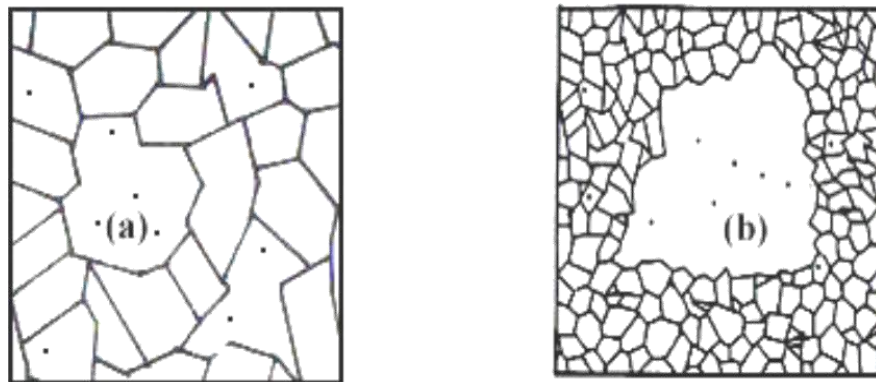


Figure 2.8: Porosity character: (a) intergranular, (b) intragranular

The porosity of ceramic samples results from two sources, intragranular porosity and intergranular porosity, Figure 2.8. An undesirable effect in ceramic samples is the formation of exaggerated or discontinuous grain growth which is characterized by the excessive growth of some grains at the expense of small, neighboring ones, Figure 2.9. When this occurs, the large grain has a high defect concentration. Discontinuous growth is believed to result from one or several of the following: powder mixtures with impurities; a very large distribution of initial

particle size; sintering at excessively high temperatures; in ferrites containing Zn and /or Mn, a low O^2 partial pressure in the sintering atmosphere. When a very large grain is surrounded by smaller ones, it is called 'duplex' microstructure. Grain boundaries begin to form at the interface between at least three contacting particles. Pores appear as voids between at least three contacting particles. Grain growth begins during the intermediate stage of sintering. Since grain boundaries are the sinks for vacancies, grain growth tends to decrease the pore elimination rate due to the increase in distance between pores and grain boundaries and by decreasing the total grain boundary surface area.

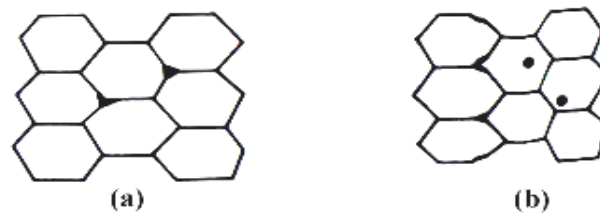


Figure 2.9: Grain growth (a) discontinuous, (b) duplex (schematic).

CHAPTER III

EXPERIMENTAL PROCEDURE

EXPERIMENTAL PROCEDURE

3.1 Rare Earth Ferrite Preparation

Rare earth ions can improve densification and increase permeability and resistivity. The preparation of rare earth ferrites with optimum desired properties is still a complex and difficult task. The rare-earth ferrite is completely defined by its chemistry and crystal structure but also requires knowledge and control of parameters of its microstructure such as density, lattice parameters, porosity and their intra- and inter-granular distribution. It is well known that almost all rare-earth ferrites decompose at the elevated temperature if want to melt them under normal conditions. In this chapter, experimental methods of sample preparation techniques of rare earth Lanthanum (La) doped Cu-Zn ferrites are described briefly. Also describe the effect of the preparation, calcinations and sintering process of the rare earth substituted Cu-Zn ferrites with the general formula $\text{Cu}_{0.15}\text{Zn}_{0.85}\text{La}_x\text{Fe}_{2-x}\text{O}_4$. The normal methods of preparation of ferrites comprise of the conventional ceramic method or powder metallurgy, chemical co-precipitation method, sol-gel method, wet method etc. In this work conventional ceramic method has been employed for the preparation of $\text{Cu}_{0.15}\text{Zn}_{0.85}\text{La}_x\text{Fe}_{2-x}\text{O}_4$ ferrites for its relative simplicity and availability.

3.2 Composition of the Studied Ferrites

In the present research several compositions of La substituted ferrites are synthesized, characterized and investigated. A series of mixed ferrites of various compositions were fabricated by solid state reaction technique keeping in view of their ionic radial and valences for maintaining the charge neutrality. The sample preparation process is sintering facility available in Solid State physics Laboratory at Khulna University of Engineering and Technology (KUET). The ferrites under investigation are:

- (i) $\text{Cu}_{0.15}\text{Zn}_{0.85}\text{Fe}_2\text{O}_4$
- (ii) $\text{Cu}_{0.15}\text{Zn}_{0.85}\text{La}_{0.02}\text{Fe}_{1.98}\text{O}_4$
- (iii) $\text{Cu}_{0.15}\text{Zn}_{0.85}\text{La}_{0.04}\text{Fe}_{1.96}\text{O}_4$
- (iv) $\text{Cu}_{0.15}\text{Zn}_{0.85}\text{La}_{0.06}\text{Fe}_{1.94}\text{O}_4$
- (v) $\text{Cu}_{0.15}\text{Zn}_{0.85}\text{La}_{0.08}\text{Fe}_{1.92}\text{O}_4$

3.3 Sample Preparation Technique

Polycrystalline ferrites with optimum desired properties are still a complex and difficult task. Ferrites with optimized properties have always demanded delicate handling and cautious approach in materials synthesis and appropriate knowledge of

thermodynamics control of the chemical composition and homogeneity. Today, the large majority of ferrite powders are made by the conventional Ceramic process or Solid State Reaction method [Kong *et. al.*, 2007]. Most non-conventional process involves producing the powder by a wet method. Among these methods, some are :

- ❖ Chemical co-precipitation[Soilah Zahi *et. al.*, 2007]
- ❖ Sol-gel synthesis[Hakim *et. al.*, 2007]
- ❖ Organic precursors
- ❖ Co-spray roasting
- ❖ Microwave Sintering Method [Bhaskar *et. al.*, 2004]
- ❖ Auto Combustion Method [Yue *et. al.*, 2001]
- ❖ Glass crystallization etc.

In the present research, we prepared our sample $\text{Cu}_{0.15}\text{Zn}_{0.85}\text{La}_x\text{Fe}_{2-x}\text{O}_4$ [Where $x = 0.00, 0.02, 0.04, 0.06$ and 0.08] by Solid state reaction technique.

3.3.1 Solid State Reaction Method

In the solid state reaction method, the required composition is usually prepared from the appropriate amount of raw mineral oxides or carbonates by crushing, grinding and milling. Solid state reaction occurs between apparently regular crystal lattices, in which the kinetic motion is very much restricted and it depends on the presence of lattice defects [Nelson and Riely 1945]. In solid state reaction method, appropriate amounts of two or more component of chemical compounds are carefully grinded together and mixed thoroughly in mortar with pestle or ball milling with appropriate homogenization. Solid oxides do not usually react together at room temperature over normal time scale and it is necessary to heat them at much higher temperatures. The ground powders are then calcined in air or oxygen at a temperature above 700°C . Sometime this process is continued until the mixture is converted into the correct crystalline phase. The calcined powders are then further crushed into fine powders. The pellets or disc shaped and toroid shaped samples are made of these calcined powders using uniaxial or iso-static pressure. Sintering is carried out in the solid state, at temperatures between $700 - 1600^\circ\text{C}$, for times of typically 1- 5 hours and in various atmospheres (e.g. Air, O_2 and N_2).

The overall preparation process generally comprised of the following four major steps are:

- ❖ Preparing a mixture of desired composition

- ❖ Pre sintering the mixture to form ferrite
- ❖ Converting the Raw ferrite into powder and pressing the powder
- ❖ Sintering.

3.4 Sample preparation

The samples were synthesized by solid state reaction method. The starting materials for the preparation of the studied composition were in the form of powder oxides of in Framat Advance Materials USA. High purity powders of CuO (99.9%), ZnO (99.9%), La₂O₃ (99.9%), Fe₂O₃ (99.9%) were used as the raw materials. The exact amounts of compounds were calculated for each composition. Using those raw materials were weighed and mixed thoroughly by hand milling. During hand milling, few drops of acetone were added to increase the degree of mixing. The mixture was pre-sintered at 800°C for 3 hours. The calcined powder again was crashed into fine powders. From the fine powders, toroid and disk-shaped samples were prepared and sintered at 1150° C for 3 hours. After sintering the sample we got the final product and studied the electrical and magnetic properties of the desired sample.

3.4.1 Calculation for sample preparation

For the polycrystalline Cu_{0.15}Zn_{0.85}La_xFe_{2-x}O₄ [where x = 0.00, 0.02, 0.04, 0.06 and 0.08] arrangement we used CuO, ZnO, La₂O₃ and Fe₂O₃. The appropriate weight percentage of the oxide to be mixed for various samples was calculated by using formula:

$$\text{Weight \% of oxide} = \frac{M.wt \cdot \text{of oxide} \times \text{required weight of the sample}}{\text{Sum of Mol.wt.of each oxide in a sample}}$$

To get exact amount of each of the compounds the detail calculations are shown in following three tables.

Table 3.1: Atomic /molecular mass of raw materials

Name of compound/atom	Molecular / Atomic mass(g/mol)
CuO	79.55
ZnO	81.39
La ₂ O ₃	325.82
Fe ₂ O ₃	159.70
Cu	63.55
Zn	65.39
La	138.91
Fe	55.85
O	16

Table 3.2: Calculation of total mass of the composition

Composition	Mass of the sample (g)
$\text{Cu}_{0.15}\text{Zn}_{0.85}\text{Fe}_2\text{O}_4$	$(63.55 \times 15) + (65.39 \times 85) + (55.85 \times 2) + (16 \times 4) = 240.815$
$\text{Cu}_{0.15}\text{Zn}_{0.85}\text{La}_{0.02}\text{Fe}_{1.98}\text{O}_4$	$(63.55 \times 15) + (65.39 \times 85) + (138.91 \times 0.02) + (55.85 \times 1.98) + (16 \times 4) = 242.475$
$\text{Cu}_{0.15}\text{Zn}_{0.85}\text{La}_{0.04}\text{Fe}_{1.96}\text{O}_4$	$(63.55 \times 15) + (65.39 \times 85) + (138.91 \times 0.04) + (55.85 \times 1.96) + (16 \times 4) = 244.137$
$\text{Cu}_{0.15}\text{Zn}_{0.85}\text{La}_{0.06}\text{Fe}_{1.94}\text{O}_4$	$(63.55 \times 15) + (65.39 \times 85) + (138.91 \times 0.06) + (55.85 \times 1.94) + (16 \times 4) = 245.799$
$\text{Cu}_{0.15}\text{Zn}_{0.85}\text{La}_{0.08}\text{Fe}_{1.92}\text{O}_4$	$(63.55 \times 15) + (65.39 \times 85) + (138.91 \times 0.08) + (55.85 \times 1.92) + (16 \times 4) = 247.460$

Table 3.3: Calculation for 20 g sample preparation

Composition	Need of CuO(g)	Need of ZnO(g)	Need of Fe ₂ O ₃ (g)	Need of La ₂ O ₃ (g)
$\text{Cu}_{0.15}\text{Zn}_{0.85}\text{Fe}_2\text{O}_4$	$(79.5 \times 0.15 \times 20) / 240.815 = 0.9911$	$(81.39 \times 0.85 \times 20) / 240.815 = 5.7457$	$(159.70 \times 20) / 240.815 = 13.2633$	N/A
$\text{Cu}_{0.15}\text{Zn}_{0.85}\text{La}_{0.02}\text{Fe}_{1.98}\text{O}_4$	$(79.5 \times 0.15 \times 20) / 242.475 = 0.9842$	$81.39 \times 0.85 \times 20 / 242.475 = 5.7063$	$(159.70 \times 1.98 \times 20) / (2 \times 242.475) = 13.0407$	$(325.82 \times 0.02 \times 20) / (2 \times 242.45) = 0.2687$
$\text{Cu}_{0.15}\text{Zn}_{0.85}\text{La}_{0.04}\text{Fe}_{1.96}\text{O}_4$	$(79.5 \times 0.15 \times 20) / 244.137 = 0.9776$	$81.39 \times 0.85 \times 20 / 244.137 = 5.6675$	$(159.70 \times 1.96 \times 20) / (2 \times 244.137) = 12.8212$	$(325.82 \times 0.04 \times 20) / (2 \times 244.17) = 0.5338$
$\text{Cu}_{0.15}\text{Zn}_{0.85}\text{La}_{0.06}\text{Fe}_{1.94}\text{O}_4$	$(79.5 \times 0.15 \times 20) / 245.799 = 0.9710$	$81.39 \times 0.85 \times 20 / 245.799 = 5.6290$	$(159.70 \times 1.94 \times 20) / (2 \times 245.799) = 12.6050$	$(325.82 \times 0.06 \times 20) / (2 \times 245.79) = 0.7954$
$\text{Cu}_{0.15}\text{Zn}_{0.85}\text{La}_{0.08}\text{Fe}_{1.92}\text{O}_4$	$(79.5 \times 0.15 \times 20) / 247.460 = 0.9640$	$81.39 \times 0.85 \times 20 / 247.460 = 5.5910$	$(159.70 \times 1.92 \times 20) / (2 \times 247.460) = 12.3910$	$(325.82 \times 0.08 \times 20) / (2 \times 247.40) = 1.0530$

3.4.2 Mixed and Milled the Samples (Hand Milling)

Samples were weighed according to the calculation and then mixed thoroughly by solid state reaction method. In these step greatly, depending on the starting materials, when component oxide are used, the corresponding step involves a mere mixing of the oxides by wet milling. To avoid Fe contamination, mixing is done hand milling and a fluid such as distilled water is used to prepare the mixture into slurry. Fe₂O₃ and MO are required are taken in powder form with the captions in the ratio corresponding to that in the final product. Each of the compositions was grinded for four hours using agate mortar and pestle. The following figure shows the hand milling set up.



Figure 3.1: Raw materials in agate mortar with pestle.

Mortar and pestle are implements used since ancient times to prepare ingredients or substances by crushing and grinding them into a fine paste or powder in the kitchen, medicine and pharmacy.

3.4.3 Pre-sintering the Mixture to form Ferrite

The powder was pre-sintered in a furnace in air atmosphere. Sample prepared after using recrushed powders from pre-sintering gives significant improved properties and good biocompatibility. The slurry prepared is dried, palletized and then transferred to a porcelain Ni-crucible for pre-sintering in a constant temperature 800°C for 3 hours. Pre-sintering of the materials was performed KSL-1700X FURNACE at Solid State Laboratory, KUET, Khulna. It is done to increase the strength green compact and remove the lubricants and binders added during blending.

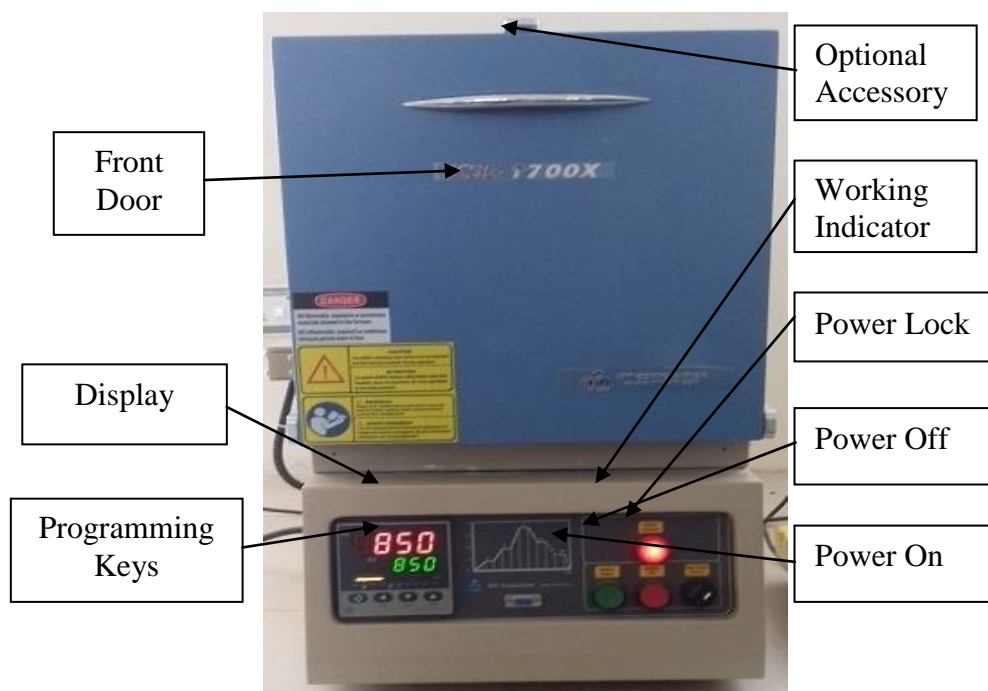
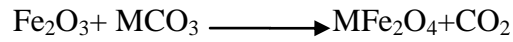
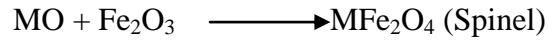


Figure 3.2: Furnace (KSL-1700X made in USA) in the solid state physics laboratory, (KUET)

The cooling and heating rates were 4°C/min. The furnace was slowly cooled to room temperature. During the Pre-sintering stage, the reaction of Fe₂O₃ with metal oxide/carbonate (say, MO or MCO₃) takes place in the solid state to form spinel according to the reactions:



3.4.4 Pressing or Extrusion



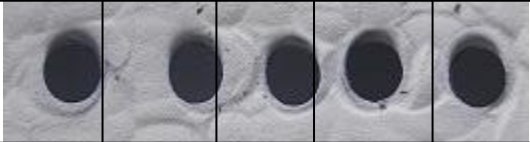

Powder pressing is the compaction of powders into a geometric form. Dry powder is mixed with an organic binder and pressed into compacts of desired shapes either by the conventional method. A binder is usually added prior to compaction, at a concentration lower than 5wt%. Binders may be used to increase compact ability.



Figure 3.3: Hydraulic press and dies for preparing sample

The most commonly used binder in ferrite is polyvinyl alcohol. The binder facilitates the particles flow during compacting and increases the bonding between the particles, presumably by forming bonds of the type particle-binder-particle. During sintering, binders decompose and are eliminated from the ferrite. Pressing is usually performed at room temperature. This creates a solid part called a green compact. The strength of this pressed, unsintered part, (green strength), is dependent on compact ability. Most shapes, such as toroidal cores, are pressed (at 1-10 ton/cm², 14-140MPa).

Table 3.4: Various Shape and size of $\text{Cu}_{0.15}\text{Zn}_{0.85}\text{La}_x\text{Fe}_{2-x}\text{O}_4$ sample

Shape	Weight (gm)	Name of the sample: $\text{Cu}_{0.15}\text{Zn}_{0.85}\text{La}_x\text{Fe}_{2-x}\text{O}_4$ [Where x=0.00, 0.02, 0.04, 0.06 and 0.08]					Purpose
		X=0.00	X=0.02	X=0.04	X=0.06	X=0.08	
Ring	1 gm						Permeability
Pellet	0.6 gm						VSM, XRD
Pellet	0.4 gm						Dielectric, Resistivity
Pellet	0.2 gm						SEM

3.4.5 Sintering

Sintering is defined as the process of obtain a dense, tough body by heating a compacted powder for a certain at a temperature high enough to significantly promote diffusion, but clearly lower than the melting point of the main component. This is very critical step in the manufacturing of ferrites. At this stage the product achieves its final magnetic and mechanical properties. Sintering is the process of compacting and forming a solid mass of material by heat or pressure without melting it to the point of liquefaction. Sintering happens naturally in mineral deposits or as a manufacturing process used with metals, ceramics, plastics, and other materials. In this process the atoms in the materials diffuse across the boundaries of the particles, fusing the particles together and creating one solid piece. Sintering process takes places without melting the sample i.e. heating the sample below its melting point. Sintering is the final step in which sintering temperature, sintering time and the atmosphere of the furnace play very important role on the magnetic property of final samples. Sintering must fulfill three requirements:

- ❖ To bond the particles together so as to impart sufficient strength to the product.
- ❖ To density the grain compacts by eliminating the pores and

- ❖ To complete the reactions left unfinished in the pre-sintering step.

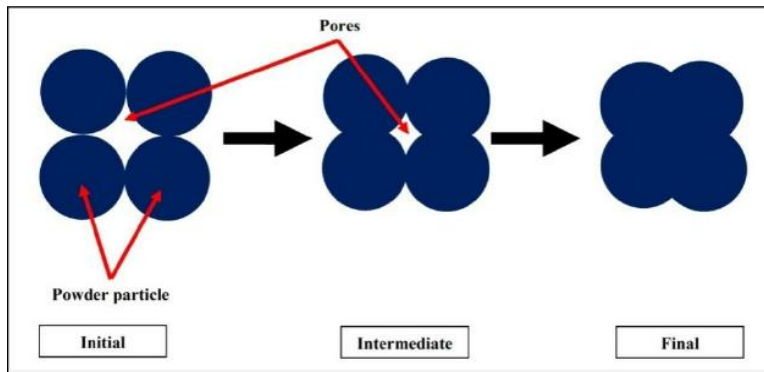


Figure 3.4: Illustration of the stages in sintering of powder particles

Sintering can be enhanced by the presence of a liquid phase. Transient liquid phase sintering occurs when the liquid phase absorbed by the solid phase during sintering. The liquid flows between the particles filling pores and causing densification by capillary action and through the provision of a fast diffusion pathway. Shrinkage occurs by particle rearrangement if the liquid volume is high enough and the green density is low enough. By the particles changing shape to allow better packing by the pore filling and by solid state sintering a solid skeleton is formed.

3.4.6 KSL-1700X-S Furnace



Figure 3.5: High Temperature Muffle Furnace (KSL-1700X-S) at Solid State Physics Laboratory, KUET

KSL-1700X-S is a compact design high temperature muffle furnace designed for maximum energy saving (<1KW at 10°C/min).It is an ideal tool for materials annealing and sintering in research laboratory.

- ❖ The furnace consists of high quality alumina fiber brick and MoSi2 heating elements with double layer case.
- ❖ Gas inlet and venting port are installed for using at oxygen or inert gas riched atmosphere.
- ❖ Design of sliding down door is for loading sample at easy.
- ❖ The furnace temperature is controlled by high precision SCR(Silicon Controlled Rectifier) digital controller with accuracy +/-1°C and 30 segments programmable up to 1700°C.

3.4.7 Illustration of Temperature Segment Setting for Sintering

The $\text{Cu}_{0.15}\text{Zn}_{0.85}\text{La}_x\text{Fe}_{2-x}\text{O}_4$ [where $x = 0.00, 0.02, 0.04, 0.06$ and 0.08] samples were sintered at 1150°C and holding time 3 hours. High Temperature Muffle Furnace (KSL-1700X-S) at Solid State Physics LabOratory, KUET was used for sintering the sample. According to the Furnace operational manual the temperature Control Program was taken with 6-segments as shown in Figure 3.6.

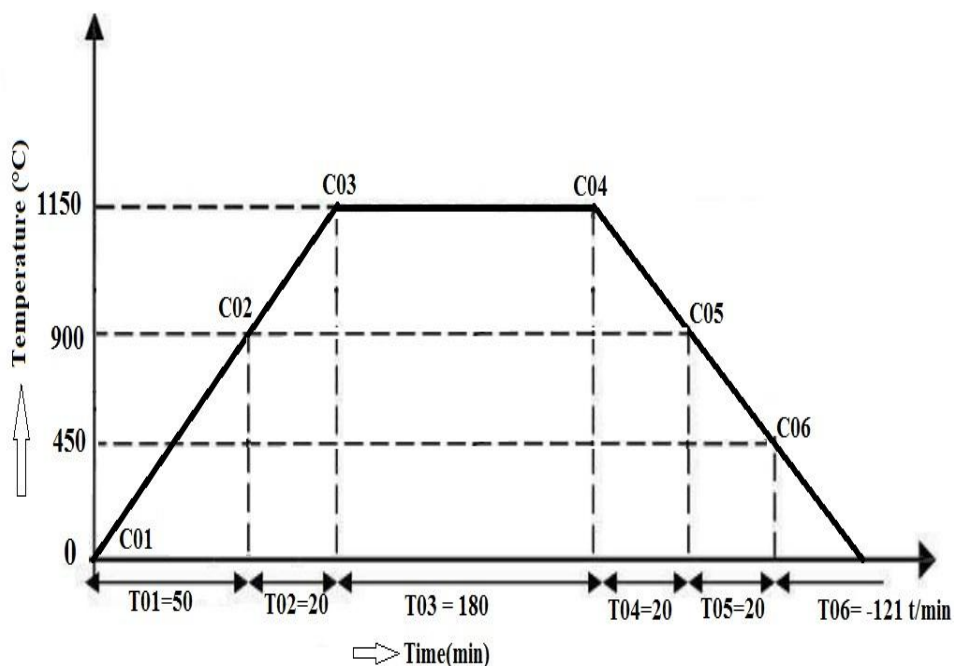
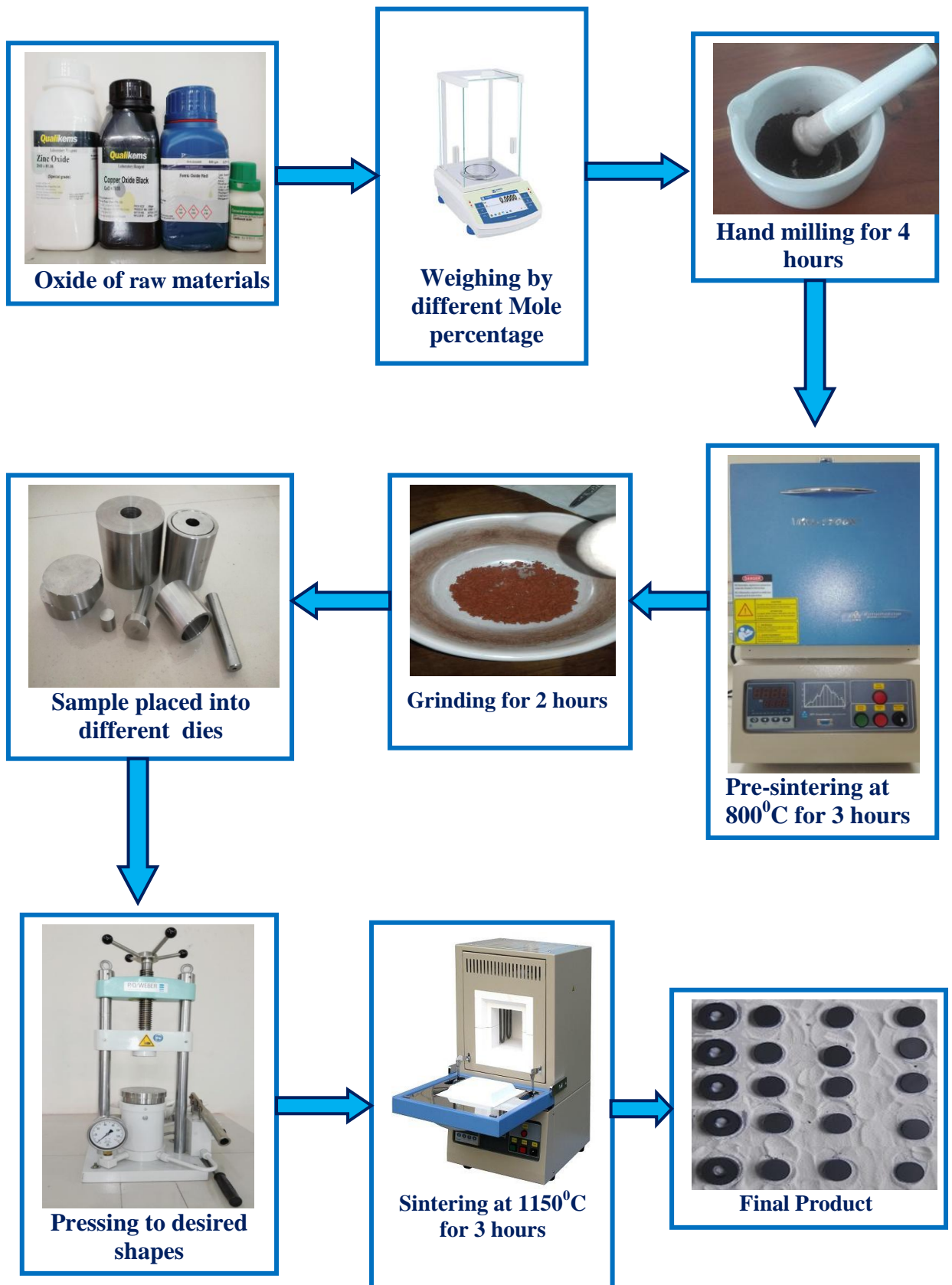


Figure 3.6: Graphical presentation of temperature control program segments

3.5 Sample Preparation at a glance



3.6 X-ray Diffraction

X-ray diffraction (XRD) is a versatile nondestructive analytical technique for identification and quantitative determination of various crystalline phases of powder or solid sample of any compound. When X-ray beam is incident on a material, the photons primarily interact with the electrons in atoms and get scattered. Diffracted waves from different atoms can interfere with each other and the resultant intensity distribution is strongly modulated by this interaction. If the atoms are arranged in a periodic fashion, as in crystals, the diffracted waves will consist of sharp interference maxima (peaks) with the same symmetry as in the distribution of atoms. Measuring the diffraction pattern therefore allows us to deduce the distribution of atoms in a material. It is to be noted here that, in diffraction experiments, only X-rays diffracted via elastic scattering are measured.

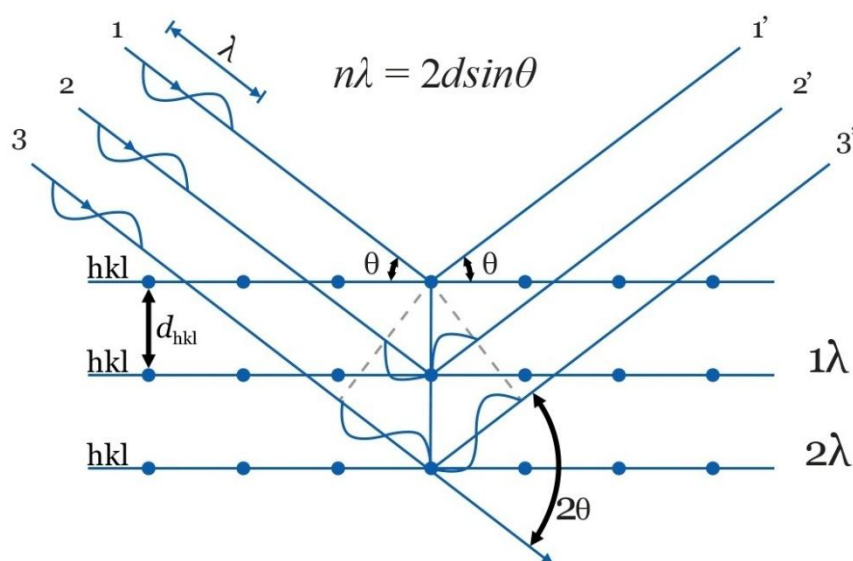


Figure. 3.7. Bragg diffraction of x-rays from successive planes of atoms.

The peaks in an X-ray diffraction pattern are directly related to the wavelength of electromagnetic radiation to the diffraction angle and the lattice spacing in atomic distance. Let us consider an incident X-ray beam interacting with the atoms arranged in a periodic manner as shown in two dimensions in Figure 3.7. The atoms, represented as spheres in the illustration, can be viewed as forming different sets of planes in the crystal. For a given set of lattice planes with an inter-plane distance of d , the condition for a diffraction (peak) to occur can be simply written as:

$$2d \sin n\theta = n\lambda \quad (3.1)$$

This is known as Bragg's law. In the equation, λ is the wavelength of the X-ray, θ is the scattering angle and n is an integer representing the order of the diffraction peak. The Bragg's law is one of the most important laws used for interpreting X-ray diffraction data. From the law, it is found that the diffraction is only possible when $\lambda < 2d$ [Cullity 1959].

3.6.1 Different Parts of the PHILIPS X'Pert PRO XRD System

A complex of instruments of X-ray diffraction analysis has been established for both materials research and specimen characterization. These include facilities for studying single crystal defects, and a variety of other materials problems. Figure 3.8 shows the inside view of the Phillips X'pert PRO XRD system .

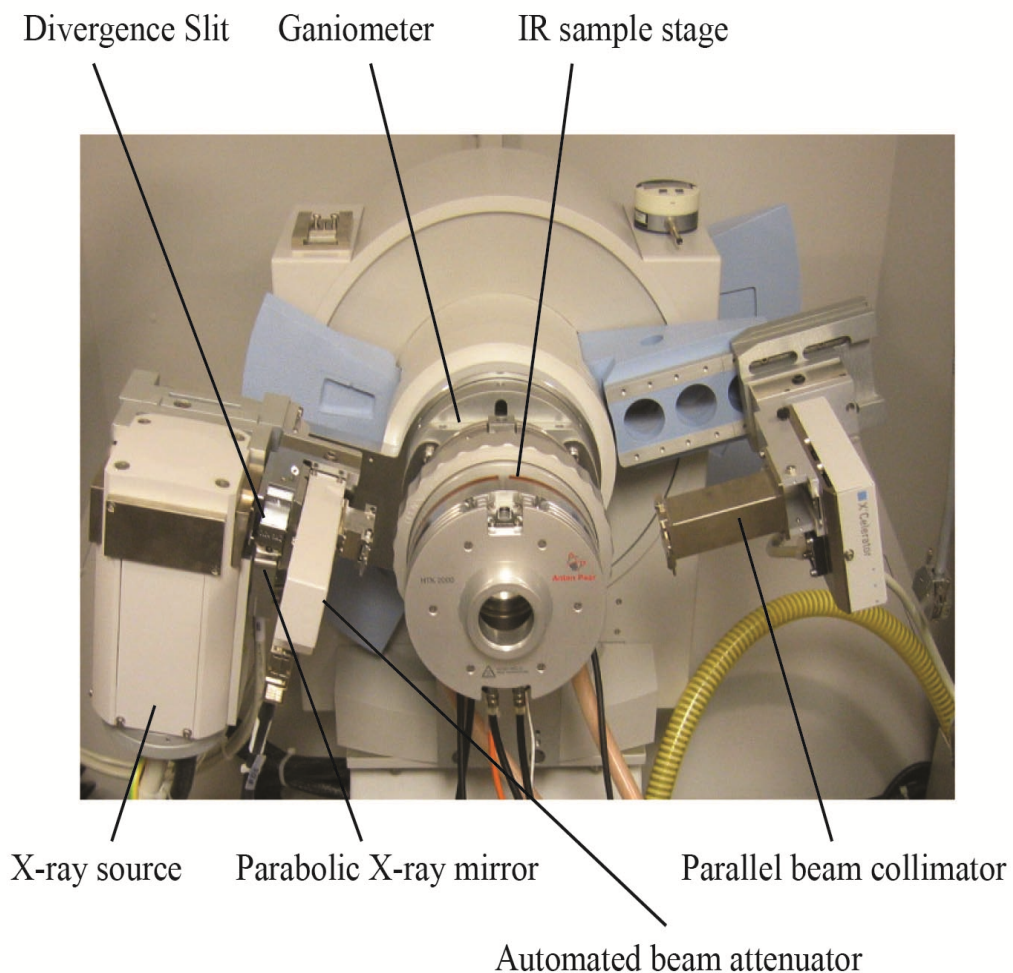


Figure 3.8: Internal arrangement of a PHILIPS X' Pert PRO X-ray diffractometer

The Phillips X' Pert PRO XRD system comprised of the following parts:

- ❖ “Cu-Tube” with maximum input power of 60 kV and 55 mA.
- ❖ “Ni- Filter” to remove Cu- K_{α} component.

- ❖ “Solar Slit” to pass parallel beam only.
- ❖ “Programmable Divergent Slits(PDS)” to reduce divergence of beam and control irradiated beam area
- ❖ “Mask” to get desired beam area
- ❖ “Sample holder” for powder sample.
- ❖ “Anti Scatter Slit (ASS)” to reduce air scattering back ground.
- ❖ “Programmable Receiving Slit (PRS)” to control the diffracted beam intensity and
- ❖ Solar Slit to stop scattered beam and pass parallel diffracted beam only.

3.6.2 Interpretation of the XRD data

The XRD data consisting of θ_{hkl} and d_{hkl} values corresponding to the different crystallographic planes are used to determine the structural information of the samples like lattice parameter and constituent phase. Lattice parameters of Cu-ferrites samples were determined. Normally, lattice parameter of an alloy composition is determined by the Debye-Scherrer method after extrapolation of the curve. We determine the lattice spacing (interplaner distance), d using these reflections from the equation which is known as Bragg’s Law.

$$2d_{hkl}\sin\theta = \lambda$$

$$\text{i.e. } d_{hkl} = \frac{\lambda}{2\sin\theta} \quad , \quad (3.2)$$

where λ is the wavelength of the X-ray, θ is the diffraction angle and n is an integer representing the order of the diffraction.

3.6.3 Lattice Parameter

The lattice parameter for each peak of each sample was calculated by using the formula:

$$a = d_{hkl} \times \sqrt{h^2 + k^2 + l^2} \quad (3.3)$$

Where h, k, l are the indices of the crystal planes. We get d_{hkl} values from the computer using software “X’ Pert HJGHS CORE”. So we got ten ‘ a ’ values for ten reflection planes such as $a_1, a_2, a_3 \dots$ etc. Determine the exact lattice parameter for each sample, through the Nelson-Riley extrapolation method. The values of the lattice parameter obtained from each reflected plane are plotted against Nelson-Riley function [Nelson and Riely 1945]. The Nelson-Riley function $F(\theta)$, can be written as,

$$F(\theta) = \frac{1}{2} \left[\frac{\cos^2 \theta}{\sin \theta} + \frac{\cos^2 \theta}{\theta} \right] \quad (3.4)$$

Where θ is the Bragg's angle. Now drawing the graph of 'a' vs. $F(\theta)$ and using linear fitting of those points will give us the lattice parameter 'a₀'. This value of 'a₀' at $F(\theta) = 0$ or $\theta = 90^\circ$. These 'a₀'s are calculated with an error estimated to be $\pm 0.0001 \text{ \AA}$.

3.6.4 X-ray Density and Bulk Density

X-ray density, ρ_x was also calculated usual from the lattice constant. The relation between ρ_x and 'a' is as follows,

$$\rho_x = \frac{ZM}{Na^3} \quad (3.5)$$

where M is the molecular weight of the corresponding composition, N is the Avogadro's number ($6.023 \times 10^{23} \text{ mole}^{-1}$), 'a' is the lattice parameter and Z is the number of molecules per unit cell, ($Z = 8$ for the spinel cubic structure). The bulk density was calculated considering a cylindrical pellet of mass (m) and volume (V) of the pellets using the relation,

$$\rho_B = \frac{\text{mass of the sample}}{\text{volume of the sample}} = \frac{m}{V} = \frac{m}{\pi r^2 h} \quad (3.6)$$

Where m is the mass of the pellet sample, r is the radius and h is the thickness of the pellet.

3.6.5 Porosity

Porosity is a measure of the empty spaces in a material. It is a parameter which is inevitable during the process of sintering of oxide materials. It is noteworthy that the physical and electromagnetic properties are strongly dependent on the porosity of the studied samples. Therefore an accurate idea of percentage of pores in a prepared sample is prerequisite for better understanding of the various properties of the studied samples to correlate the microstructure property relationship of the samples under study.

The porosity of a material depends on the shape, size of grains and on the degree of their storing and packing. The difference between the bulk density ρ_B and X-ray density ρ_x gave us the measure of porosity. Percentage of porosity has been calculated using the following relation[Smith and Wijn 1959]:

$$P = \left(1 - \frac{\rho_B}{\rho_x} \right) \times 100\% \quad (3.7)$$

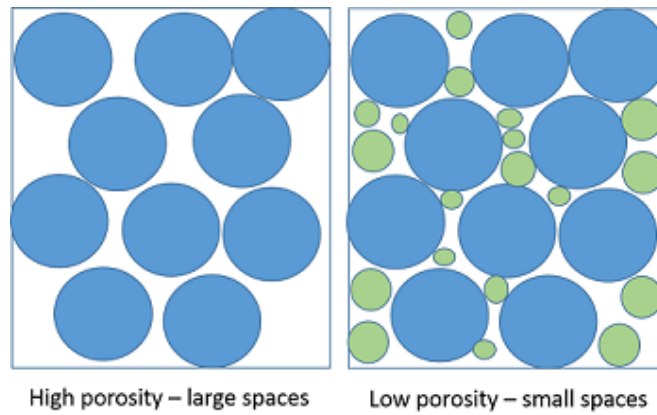


Figure 3.9: Porosity

3.7 Surface morphology and microstructure

The microstructural study was performed in order to have an insight of the grain structures. The samples of different compositions were chosen for this purpose. The samples were visualized under a High-resolution Scanning Electron Microscope (SEM) images. Average grain sizes of the samples were determined from SEM micrographs by linear intercept technique [Hossain 1998]. To do this, several random horizontal and vertical lines were drawn on the micrographs. Therefore, we counted the number of grains intersected and measured the length of the grains along the line traversed. Finally the average grain size was calculated.

3.7.1 Scanning Electron Microscope (SEM)

Scanning Electron Microscope (SEM) is a type of electron microscope that produces images of a sample by scanning the surface with a focused beam of electrons. SEM is detecting signals from the interaction of the incident electron with the sample's surface. In Scanning Electron Microscope process signals come from the primary beam impinging upon the sample and from other interactions within the sample near the surface. The SEM is capable of producing high resolution images of a sample surface in its primary use mode, secondary electron imaging. Characteristic x-rays are emitted when the primary beam causes the ejection of inner shell electrons from the sample and are used to tell the elemental composition of the sample. The back-scattered electrons emitted from the sample may be used alone to form an image.



Figure 3.10: Scanning Electron Microscope (SEM)

3.8 Vibrating Sample Magnetometer (VSM)

A vibrating Sample Magnetometer (VSM) is a scientific instrument that measures magnetic properties. It operates on the Faraday's law of induction. The working principle of VSM is the measurement of the electromotive force induced by a magnetic sample when it is vibrated at a constant frequency in the presence of a static and uniform magnetic field.

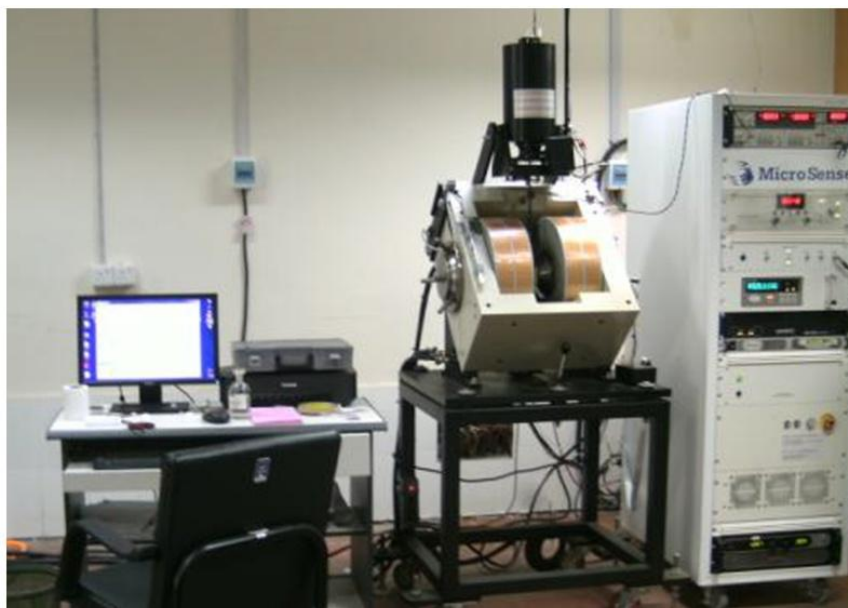


Figure 3.11: Vibrating Sample Magnetometer

In a VSM, a sample is placed within a uniform magnetic field H which induces a magnetization M in the sample. It is then vibrated sinusoidally, which creates a corresponding vibration of the magnetic flux in the pick-up coils nearby and induces a sinusoidal voltage. The amplitude of the ac voltage is proportional to the samples magnetic moment and measured by a lock-in amplifier. In this study, Microsense VSM model EV7 at Atomic Energy Commission, Dhaka was used to determine the magnetic properties of the samples. A small part of the samples (9 -11 mg) were used and was made to avoid movements inside the sample holder. To understand the ferromagnetic effect, full-cycle hysteresis loops were obtained over a wide range of field from -10 KOe to +10 KOe.

3.8.1 Working Procedure of Vibrating Sample Magnetometer

If a sample is placed in a uniform magnetic field, created between the poles of an electromagnet, a dipole moment will be induced. If the sample vibrates with sinusoidal motion a sinusoidal electrical signal can be induced in suitable placed pick-up coils. The signal has the same frequency of vibration and its amplitude will be proportional to the magnetic moment, amplitude, and relative position with respect to the pick-up coils system. Figure 3.12 shows the block diagram of vibrating sample magnetometer.

The sample is fixed to a sample holder located at the end of a sample rod mounted in an electromechanical transducer. The transducer is driven by a power amplifier which itself is driven by an oscillator at a frequency of 90 Hz. So, the sample vibrates along the Z axis perpendicular to the magnetizing field. The latter induce a signal in the pick-up coil system that is fed to a differential. The output of the differential amplifier is subsequently fed into a tuned amplifier and an internal lock in amplifier that receives signal supplied by the oscillator.

The output of this lock-in amplifier, or the output of the magnetometer itself, is a DC signal proportional to the magnetic moment of the sample being studied. The electromechanical transducer can move along X, Y and Z directions in order to find the saddle point. Calibration of the vibrating sample magnetometer is done by measuring the signal of a pure Ni standard of known saturation magnetic moment placed in the saddle point. The basic instrument includes the electromechanical system and the electronic system (including a personal computer). Laboratory electromagnets or superconducting coils of various maximum field strengths may be used.

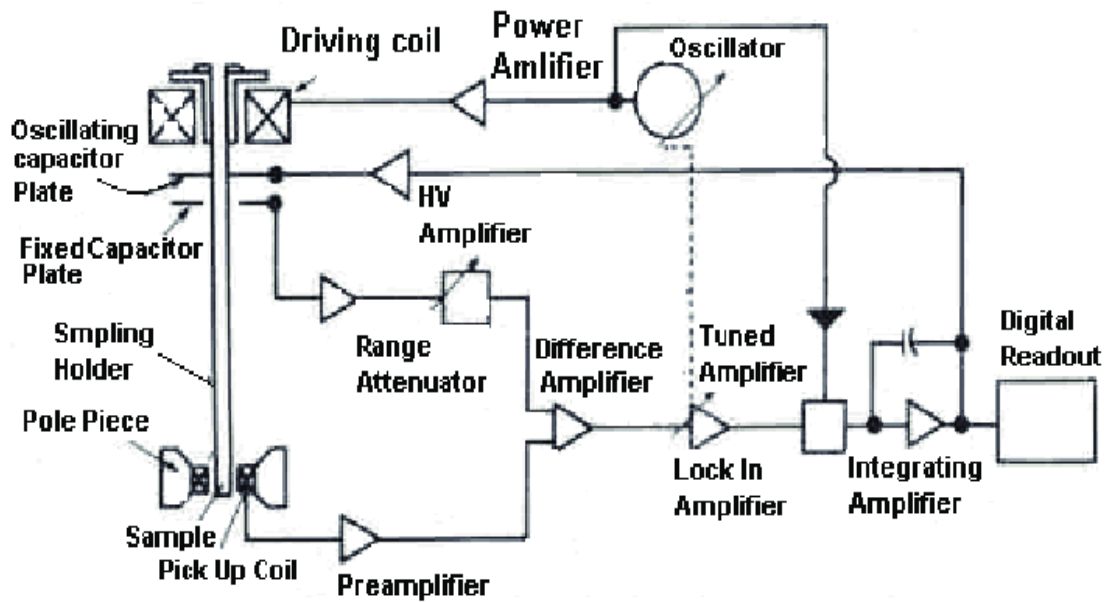


Figure 3.12: Block diagram of vibrating sample magnetometer.

3.9 Permeability Measurement

3.9.1 Wayne Kerr Precision Impedance Analyzer

The Wayne Kerr Technologies 6500B series of Precision Impedance analyzer provides impedance measurement capability of components from 20Hz up to 120 MHz. A comprehensive range of functions enables a component to be accurately characterized over a wide frequency range with a choice of Analysis and meter modes allowing swept, single and repetitive measurements. The Graphical User Interface(GUI) combined with the large touch screen TFT display enables measurement parameters to be modified easily and quickly Fig: 3.10. The instrument may be remotely controlled using the GPIB or LAN interface.

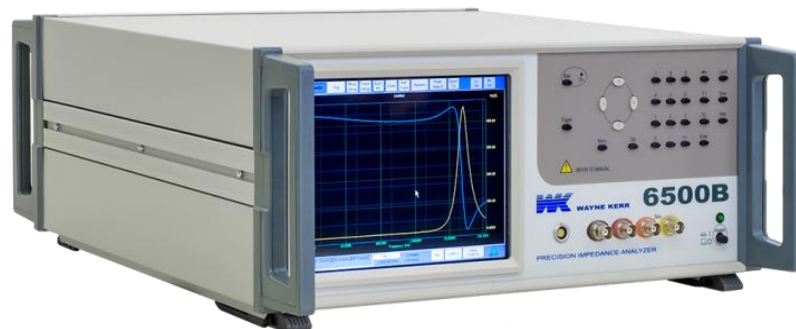


Figure 3.13: Wayne Kerr Impedance analyzer (6500B series) in Solid State Laboratory, Physics, KUET

A comprehensive range of AC functions enables a wide range of components to be measured accurately. Each measurement displays two user selectable components, which allow specific component characteristics to be monitored. Any of the following parameters can be measured and displayed.

Table 3.5

AC Measurement parameters	
❖	Impedance (Z)
❖	Inductance (L)
❖	Resistance (R)
❖	Capacitance (C)
❖	Phase Angle (θ)
❖	Dissipation Factor (D)
❖	Quality Factor (Q)
❖	Reactance (X)
❖	Conductance (G)
❖	Susceptance (B)
❖	Admittance (Y)



Figure 3.14: Complex permeability measurement by Wayne Kerr Precision Impedance analyzer

3.9.2 Permeability

The measurements of complex permeability of the toroid shaped samples were performed at room temperature in the frequency range from 1 KHz to 100MHz. To determine the frequency dependent complex permeability of the studied samples, toroid shape samples were used. The polished samples were cleaned with acetone and then coiled with copper wire. The real part, μ' and imaginary part, μ'' of the complex permeability were measured using the following formulas,

$$\mu' = \frac{L_S}{L_0} \quad (3.8)$$

$$\text{and } \mu'' = \mu' \cdot \tan \delta_M \quad (3.9)$$

Here, L_S is the inductance of the sample and $L_0 = \frac{\mu_0 N^2 S}{\pi d}$ derived theoretically for the samples. L_0 is the inductance of the winding coil except the sample, N represents the

number of turns of the coil ($N = 5$), S indicates the cross sectional area of the toroid samples as given below,

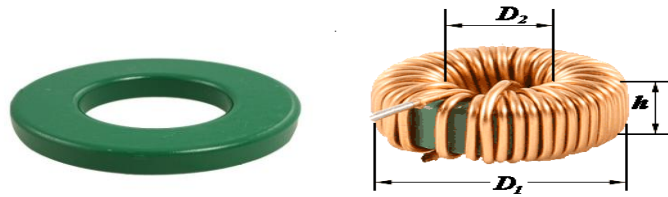


Figure 3.15: Toroid sample with winding coil.

$$S = d \times h \quad (3.10)$$

$$\text{and, } d = \frac{d_2 - d_1}{2} \quad (3.11)$$

Where, d_1 is the inner radius, d_2 is the outer radius and h is the height of the ring. Again, \bar{d} indicates the mean diameter of the toroidal sample and can be written as,

$$\bar{d} = \frac{d_1 + d_2}{2} \quad (3.12)$$

Again, Quality Factor

$$Q = \frac{1}{\tan \delta_M} \quad (3.13)$$

And relative quality factor

$$\text{RQF} = \frac{\epsilon'}{\tan \delta_M} \quad (3.14)$$

3.10 Dielectric Properties

Ceramics are mostly covalently bonded material hence electrically non conductive or insulator. Importance of particular property depends on the application demand. For instance, dielectric strength is an important parameter for application of ceramic as insulators used in power transmission line, load bearing general insulators, in house hold appliances etc. In this kind of applications where frequency do not exceed 1kHz, the break down strength, measured in kV/cm, together with mechanical strength are important factors. The dielectric constant (ϵ') or loss factor (ϵ'') does not matter much. On the other hand, for capacitors and electronics application just the opposite required. The values of ϵ' and ϵ'' are of prime importance, not only their room temperature values but also as function of frequency. These are intrinsic properties of material; especially of polycrystalline ceramic can be modified by doping, micro structural variation.

3.10.1 Dielectric Constant

Dielectric constant measurements were done by using Wayne Kerr Impedance Analyzer 6500B. The overall dielectric constant (ϵ') of an insulator material as given by the relation:

$$D = \epsilon_0 E = \epsilon_0 \epsilon' E \quad (3.15)$$

where, D represents the electric displacement, E the electric field in the dielectric, ϵ' the dielectric constant and ϵ_0 permittivity of the vacuum. The dielectric constant ϵ' is an intrinsic property of a material and a measure of the ability of the material to store electric charge relative to vacuum. It is measured directly from the capacitance of a capacitor in which the material is used as electrode separator or dielectric. The capacitive cell, the dielectric constant (ϵ'), total charge (q) and capacitance © can be developed as follows:

$$\epsilon' = \frac{D}{\epsilon_0 E} = \frac{\frac{Q}{A}}{\frac{\epsilon_0 V}{d}} \quad (3.16)$$

$$\therefore Q = \frac{\epsilon_0 \epsilon' A V}{d} = C V \quad (3.17)$$

Where,
$$C = \frac{\epsilon_0 \epsilon' A}{d} \quad (3.18)$$

Here A represents the area of the capacitive cell, d its thickness, C is the capacitance of the material, V the voltage across the cell and $\epsilon_0 \left(\frac{F}{m} \right)$ the material permittivity in vacuum.

Thus ϵ' represents the ratio of the permittivity or charge storage capacity relative to air or vacuum as dielectric,

$$\epsilon' = \frac{cd}{\epsilon_0 A} \quad (3.19)$$

where c is the capacitance of the pellet in Farad, d the thickness of the pellet in meter, A the cross-sectional area of the flat surface of the pellet in m^2 and ϵ_0 the constant of permittivity for free space. Dielectric measurement as a function of frequency in the range 100Hz-120MHz at room temperature were carried out by using Wayne Kerr Impedance Analyzer 6500B in conjunction with a laboratory made furnace which maintain the desired temperature with the help of a temperature controller.

3.10.2 Dielectric Loss

Dielectric loss often attributed to ion migration, ion vibration & deformation and electric polarization. Ion migration is particularly important and strongly affected by temperature and frequency. The losses due to ion migration increase at low frequency and the temperature increases. By definition,

$$\tan\delta = \frac{\epsilon''}{\epsilon'} \quad (3.20)$$

The imaginary part of dielectric constant (ϵ'') of the sample was calculated using relation: $\epsilon'' = \epsilon' \tan\delta$; where $\tan\delta$ is the dielectric loss tangent.

3.11 DC resistivity

Sintered pellet specimens were used to determine resistivity. Electrical conductivity of the samples was studied after silver pasting the two polished surfaces of each pellet as shown in Figure 3.15. The temperature dependent ρ_{DC} from room temperature up to 500K were carried out by using two probe method and was estimated by using the following relation

$$\rho_{DC} = \frac{R\pi r^2}{l} \quad (3.21)$$

Where R is the resistance, r is the radius and l is the thickness of the samples.

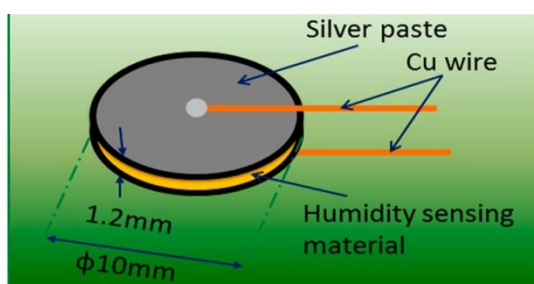


Figure 3.16: Schematic arrangement on the silver pasted pellet sample

CHAPTER IV

RESULTS AND DISCUSSION

RESULTS AND DISCUSSION

4.0 Introduction

Now days the rare-earth oxides are becoming promising additives to change the magnetic properties of ferrites. The investigation studied the effect of rare-earth metals substitution on the properties of Cu-Zn ferrites. Different substitutions into soft ferrites have been incorporated to get electrical and magnetic properties [Ajmal and Maqsood 2008, Mondal 2018, Hossain 2017]. It is well known that almost all rare-earth ferrites decompose at the elevated temperature if want to melt them under normal conditions. Polycrystalline spinel ferrites present an important set of properties such as permeability used in the radio frequency level, high Curie temperature, high electrical resistivity, low dielectric losses, low cost and environmental stability [Ovidiu F. Caltun, Leonard Spinu July 2001]. Spinel is an important class of mixed-metal oxides has the general chemical composition of AB_2O_4 . Normally A is divalent atom of radius $72A^\circ$ is Cu^{2+} , $0.82A^\circ$ is Zn^{2+} and B is a trivalent atom of radius La^{3+} is $1.17A^\circ$, Fe^{3+} is $64A^\circ$. Physical, electrical and magnetic properties arise from the ability of ferrites to distribute the cations among the available A and B sites. In this chapter, magnetic, electrical and structural properties of Lanthanum (La) doped Cu-Zn ferrites are investigated. The La substituted polycrystalline $Cu_{0.15}Zn_{0.85}La_xFe_{2-x}O_4$ [where $x = 0.00, 0.02, 0.04, 0.06$ and 0.08] have been prepared by standard solid state reaction technique. All the samples show crystallization with we defined diffraction patterns exhibited that all the samples were identified as a single phase of cubic spinel structure. The magnetic properties such as complex permeability of the ferrites investigated in the frequency range (1 KHz to 120 MHz) by Wayne Kerr Impedance Analyzer. Surface morphology was measured by SEM (model JEOL JSM 7600F) and hysteresis loop was analyzed by VSM. Dielectric properties, DC resistivity and other electrical properties of the samples are also studied.

4.1 X-Ray Diffraction Analysis of $Cu_{0.15}Zn_{0.85}La_xFe_{2-x}O_4$ Ferrites

X-ray diffraction (XRD) is a rapid analytical technique primarily used for phase identification of a crystalline material and can provide information on unit cell dimensions. It is also a common technique for the study of crystal structures and atomic spacing. XRD studies of the samples were performed by using Philips X'pert

PRO X-ray diffractometer. For XRD analysis we used powder sample $\text{Cu}_{0.15}\text{Zn}_{0.85}\text{La}_x\text{Fe}_{2-x}\text{O}_4$ of ferrites sintered at 1150°C for holding time 3 hours. In this case, X-ray diffractometer equipped with CuK_α radiation ($\lambda = 1.5418 \text{ \AA}$) in the range of $2\theta = 20^\circ$ to 65° in steps of 0.02° .

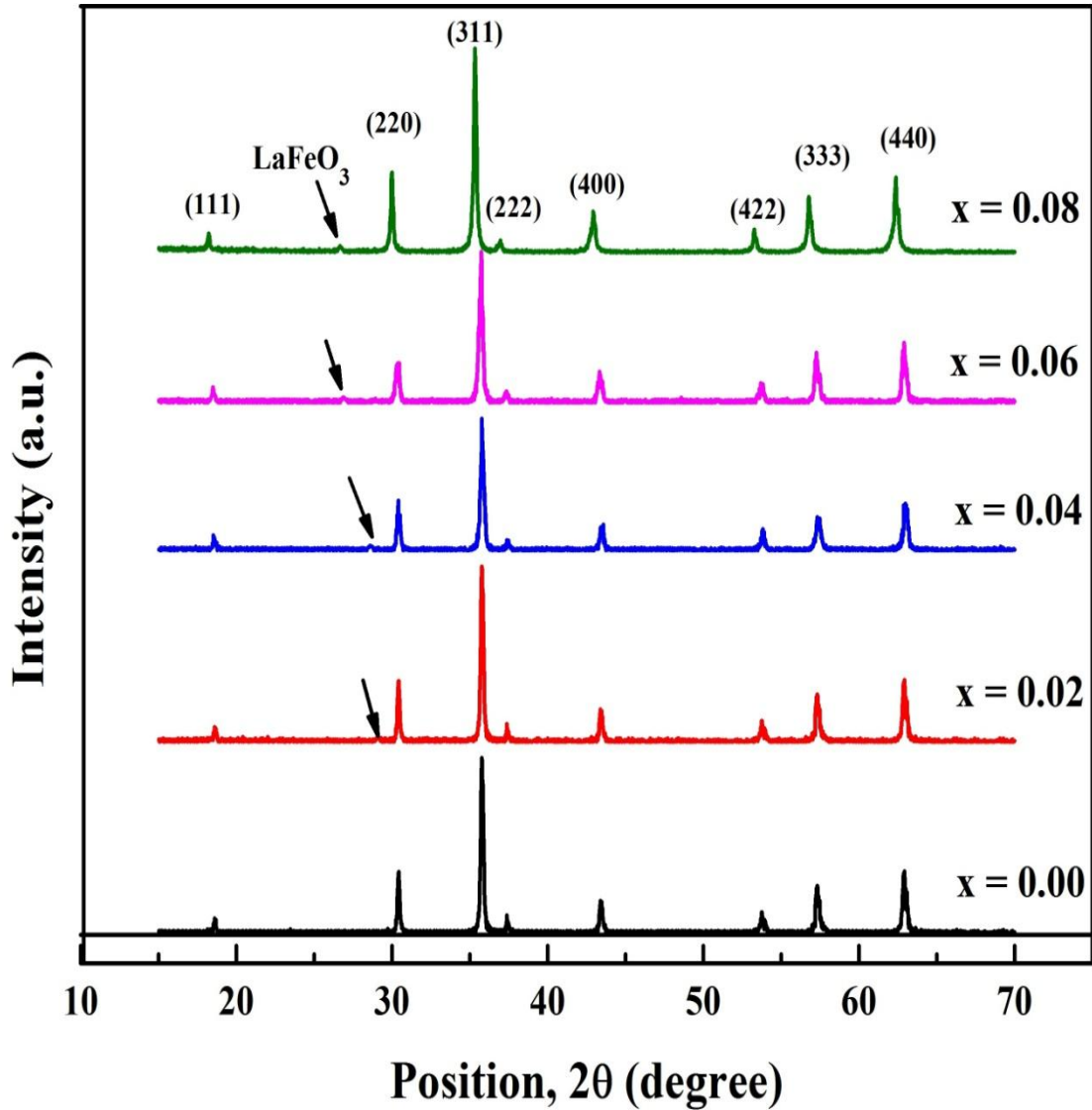


Figure 4.1: X-ray diffraction spectra of $\text{Cu}_{0.15}\text{Zn}_{0.85}\text{La}_x\text{Fe}_{2-x}\text{O}_4$, [where $x = 0.00$, 0.02 , 0.04 , 0.06 and 0.08] ferrites sintered at 1150°C for 3 hours holding time

4.1.1 Phase Analysis

The structural view of Lanthanum doped Cu-Zn ferrites was confirmed from XRD analysis. The La substituted $\text{Cu}_{0.15}\text{Zn}_{0.85}\text{La}_x\text{Fe}_{2-x}\text{O}_4$ [where $x = 0.00$, 0.02 , 0.04 , 0.06 and 0.08] ferrites were widely characterized by XRD shown in Figure 4.1. All the samples show crystallization with we defined diffraction patterns exhibited that all

the samples were identified as a single phase of cubic spinel structure. The XRD patterns for all the samples were indexed for fcc spinel structure and the Bragg planes are shown in the patterns. The peaks (111) (220), (311), (222), (400), (422), (333) and (440) correspond to spinel phase which are characteristic model of spinel structures with a single phase. Here, all the miller indices of a peak are either all odd or even, which confirmed that the samples are spinel lattice with cubic structure. This also confirms the homogeneity of the studied samples. All the reflection peaks were identified and indexed in good agreement.

However, a very weak reflection peak seen at $2\theta = 29.08^\circ$, $2\theta = 28.60^\circ$, $2\theta = 26.92^\circ$, $2\theta = 26.70^\circ$ is flowed to for $x = 0.02$, 0.04 , 0.06 and 0.08 respectively is more prominent indicated by the arrow with increasing La content. This peak is identified as the weak reflection peak of the LaFeO_3 phase. From the X-ray data we calculated the position of any peaks and using Bragg's law ($2d \sin \theta = n\lambda$) we got the values of interplanar spacing (d). The position of the X-ray peaks and their corresponding miller indices for the studied samples investigated are given in Table 4.1.

Table 4.1: Position of the X-ray peaks and corresponding miller indices for, $\text{Cu}_{0.15}\text{Zn}_{0.85}\text{La}_x\text{Fe}_{2-x}\text{O}_4$ [where $x = 0.00, 0.02, 0.04, 0.06$ and 0.08] ferrites

Content	Miller indices of the X-ray peaks and their position 2θ in degree							
	(111)	(220)	(311)	(222)	(400)	(422)	(333)	(440)
X=0.00	18.58	30.42	35.71	37.35	43.38	53.72	57.31	62.94
X=0.02	18.61	30.39	35.77	37.37	43.33	53.79	57.33	62.92
X=0.04	18.52	30.36	35.79	37.46	43.53	53.83	57.35	63.01
X=0.06	18.49	30.34	35.70	37.35	43.33	53.73	57.24	62.91
X=0.08	18.18	29.93	35.29	36.94	42.92	53.22	56.72	62.39

4.1.2 Lattice Parameters $\text{Cu}_{0.15}\text{Zn}_{0.85}\text{La}_x\text{Fe}_{2-x}\text{O}_4$ of Ferrites

The calculated values of exact lattice parameter for each plane with help of Nelson-Riley extrapolation method from the equation (3.4). For each of the reflection plane we got individual $F(\theta)$ and individual lattice parameter (a). Figure 4.2 shows the representative curves for Lanthanum content of extrapolating N-R function. The lattice parameter (a_0) decreases initially La doped in Cu-Zn ferrites due to the replacement of Zn^{2+} ions (radius = 0.68\AA) by the larger La^{3+} ions (radius = 1.03\AA) in the octahedral sites shown in Table-4.2.

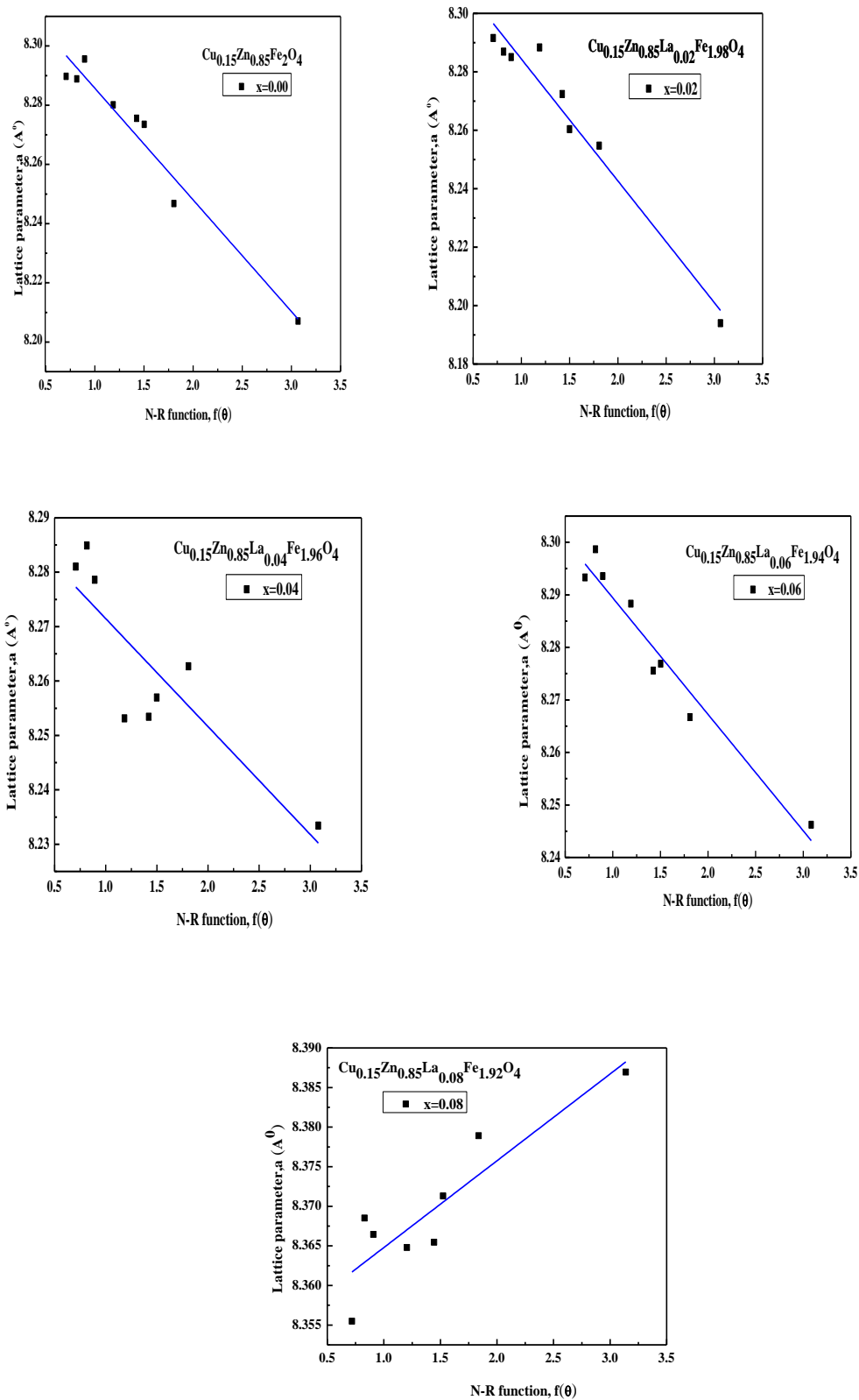


Figure 4.2: Variation of lattice parameter 'a' with N-R function and determination of exact lattice parameter 'a' of $\text{Cu}_{0.15}\text{Zn}_{0.85}\text{La}_x\text{Fe}_{2-x}\text{O}_4$ ferrites

The decrease in ‘ a_0 ’ is probably due to a distribution in the spinel lattice because of the relatively large radius of La^{3+} . This is evidence by the appearance of the minor FeLaO_3 phase, besides the major spinel phase. These changes in lattice parameters with La content indicate that the present system obeys the Vegard’s law [Vagards 1921] partially. The least square linear fitting gives the precise lattice parameter as an intercept on the Y-axis.

From each graph between lattice parameter and N-R function we got five Average values of lattice parameter for five ferrite samples. The variation of the lattice parameter as a function of La^{3+} content x is shown in Figure 4.3. Initial lattice parameter slightly decrease with increasing La content x up to 0.04 after ≥ 0.04 increasing lattice parameter. It is known that the replacement of cations by larger ones in the spinel lattice causes an increase in the lattice parameter. The initially decrease in ‘ a ’ between $x = 0.02$ and 0.04 is probably due to distortion in the spinel lattice because of the relatively large radius of La^{3+} . This is evidence by the appearance of the minor FeLaO_3 phase at $x = 0.02$ and 0.04, beside the major spinel phase. The values of lattice parameters for various $\text{Cu}_{0.15}\text{Zn}_{0.85}\text{La}_x\text{Fe}_{2-x}\text{O}_4$ ferrites are listed in Table 4.2. These changes in ‘ a ’ with La content indicates that the present system obeys the vegard’s law partially.

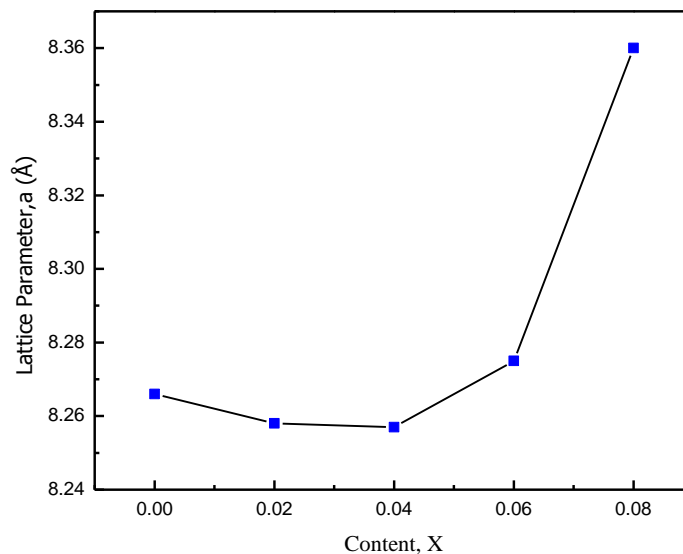


Figure 4.3: Variation of lattice parameters with the increase of La content.

4.1.3 Density and Porosity

Higher value of the permeability of the soft ferrite and higher value of coercivity of the hard magnetic materials could be achieved by controlling the density. The X-ray density calculated from the determined lattice parameter and bulk density measured from the ratio of mass and volume of all the $\text{Cu}_{0.15}\text{Zn}_{0.85}\text{La}_x\text{Fe}_{2-x}\text{O}_4$ ferrite samples. The calculated values of the X-ray density (ρ_x), bulk density (ρ_B) and porosity (P) of the present ferrites are listed in Table- 4.2. The X-ray density or theoretical density ρ_x was found to be slight decrease with the increasing in La^{3+} substitution. This may be related to the molecular weight (M) and lattice constant (a). The increase in X-ray density may be due to the higher atomic mass of La^{3+} (138.91 amu) than that of Fe^{3+} (55.85 amu). On the other hand, bulk density increases with increase of La content. Porosity also increased with the increasing of La content up to $x = 0.04$ but after ≥ 0.04 slight decreases shown in Table 4.2. It was difficult to remove these closed porosity due to the evaporation of constituents specially Zn^{2+} ions.

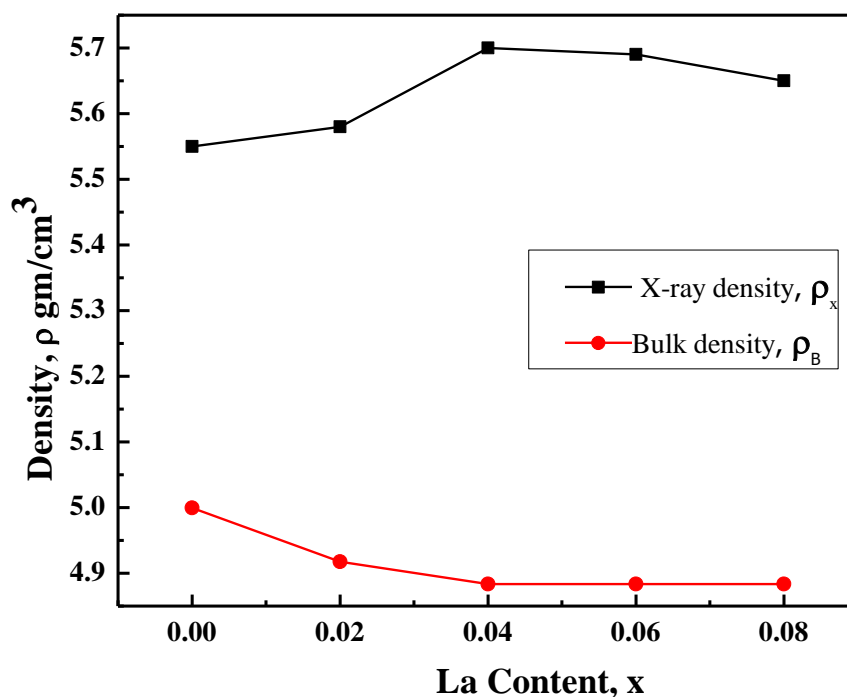


Figure 4.4: Variation of bulk density and X-ray density as a function of La content

It is observed that bulk density is lower than the X-ray density shown in Figure 4.4. This may be due to the existence of pores which were formed and developed during the sample preparation or sintering process. This may be porosity or voids into the samples are not considered in the X-ray density. In this case imaginary mass is considered instead of real mass. Other hand bulk density real mass and dimensions are taken. Therefore the bulk density is lower than that of X-ray density.

Table 4.2: Data of the lattice parameter (a), X-ray density (ρ_x), bulk density (ρ_B), porosity (P%) of $\text{Cu}_{0.15}\text{Zn}_{0.85}\text{La}_x\text{Fe}_{2-x}\text{O}_4$, [Where $x=0.00, 0.02, 0.04, 0.06$ and 0.08] ferrites sintered at 1150°C for 3 hours

La Content in x	'a' in (Å)	Bulk density, ρ_B (gm/cm^3)	X-ray density, ρ_x (gm/cm^3)	Porosity (%)
0.00	8.266	4.99	5.55	9.92
0.02	8.258	4.91	5.58	11.87
0.04	8.257	4.88	5.7	14.33
0.06	8.275	4.88	5.69	14.18
0.08	8.360	4.88	5.65	13.58

It is known that the porosity of the samples come from two sources, intragranular porosity and intergranular porosity. The intergranular porosity mainly depends on the grain size [Yang *et. al.* 2006]. At higher sintering temperatures the density is decreased because the intergranular porosity is increased resulting from discontinuous grain growth. The porosity which is intrinsic for any oxide material plays an important role in the deciding the magnetic and electrical properties due to pore spaces.

4.2 Microstructures of $\text{Cu}_{0.15}\text{Zn}_{0.85}\text{La}_x\text{Fe}_{2-x}\text{O}_4$ Ferrites

Magnetic properties of the samples are strongly dependent upon the sensitive control of the microstructure. Figure 4.5(a, b, c, d, e) shows a set of microstructure where the sample (a) $x = 0.00$ shows the presence of a monophasic spinel phases whereas, the La substituted materials whose (b) $x = 0.02$, (c) $x = 0.04$, (d) $x = 0.06$ and (e) $x = 0.08$ show a multiphasic microstructure consisting of a bigger matrix of ferrite grains and a smaller LaFeO_3 secondary phase at the grain junction boundaries.

The grain size of ferrite matrix phase as well as the LaFeO_3 phase decreased with increasing the La^{3+} substitutions. The crystal grain growth depends on grain boundaries migrating and larger crystal grains swallowing the small ones. Grain growth is closely related to the grain boundary mobility.

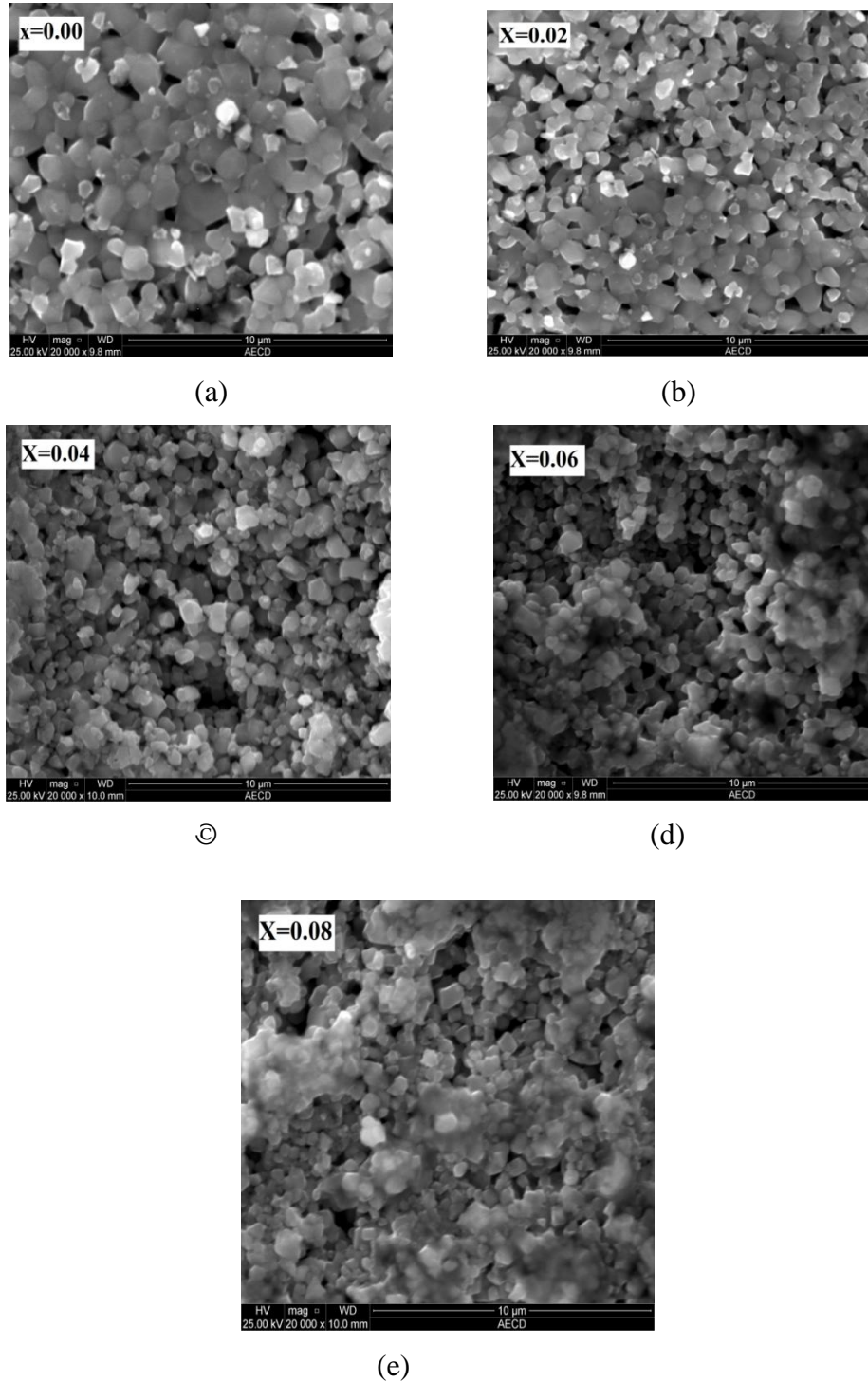


Figure 4.5: Variation of SEM micrographs with La contents (x) of $\text{Cu}_{0.15}\text{Zn}_{0.85}\text{La}_x\text{Fe}_{2-x}\text{O}_4$ ferrites where (a) 0.00, (b) 0.02, (c) 0.04, (d) 0.06 and (e) 0.08 sintered at 1150°C holding time 3hours.

Recrystallization and grain growth involve the movement of grain boundaries. It facilitates the grain growth by increasing the rate of cations inter diffusion as a result of its segregation to the grain boundaries [Mendelson 1969]. The behavior of grain growth reflects the competition between the driving force for grain boundary movement and the retarding force that drives the grain boundaries to grow over pores, thereby decreasing the pore volume and making the material dense. From these above figures can seen that the grain size decreases gradually with increasing La content. The average grain size was calculated using Image J software from the SEM micrograph and has been shown in Table 4.3. The strength of the driving force depends upon the diffusivity of individual grains, sintering temperature and porosity. Grain growth kinetics depends strongly on the impurity content. Minor dopant La can drastically change the nature and concentration of defects in the matrix, affecting grain boundary motion, pore mobility and the effect of a given dopant depends on its valence and solubility with respect to host material Fe.

Table 4.3: Average grain size for $\text{Cu}_{0.15}\text{Zn}_{0.85}\text{La}_x\text{Fe}_{2-x}\text{O}_4$ ferrites

Name of the sample	Contents	Average grain size in nm
$\text{Cu}_{0.15}\text{Zn}_{0.85}\text{Fe}_2\text{O}_4$	x = 0.00	1600
$\text{Cu}_{0.15}\text{Zn}_{0.85}\text{La}_{0.02}\text{Fe}_{1.98}\text{O}_4$	x = 0.02	1230
$\text{Cu}_{0.15}\text{Zn}_{0.85}\text{La}_{0.04}\text{Fe}_{1.96}\text{O}_4$	x = 0.04	860
$\text{Cu}_{0.15}\text{Zn}_{0.85}\text{La}_{0.06}\text{Fe}_{1.94}\text{O}_4$	x = 0.06	650
$\text{Cu}_{0.15}\text{Zn}_{0.85}\text{La}_{0.08}\text{Fe}_{1.92}\text{O}_4$	x = 0.08	580

Here the average grain size was estimated is 1600nm without La content and 1230 to 580nm with doped La in $\text{Cu}_{0.15}\text{Zn}_{0.85}\text{La}_x\text{Fe}_{2-x}\text{O}_4$ ferrites. The crystal grain growth depends on grain boundaries migrating and larger crystal grains swallowing the small ones. Grain growth is closely related to the grain boundary mobility. However, the surface morphology was found to be changed from granular to lamellar.

4.3 Magnetic Properties

4.3.1 Hysteresis loop analysis

The magnetic measurements of the $\text{Cu}_{0.15}\text{Zn}_{0.85}\text{La}_x\text{Fe}_{2-x}\text{O}_4$ [Where x=0.00, 0.02, 0.04, 0.06 and 0.08] samples at room temperature 300K were measured using

vibrating sample magnetometer (VSM) in the range of magnetic field $H = 0$ to 10kOe . From the VSM measurements, magnetization versus magnetic field ($M - H$) curves is plotted for all samples as shown in Figure 4.6. It is observed that the magnetization increases sharply at very low field ($H < 1\text{ kOe}$) which corresponds to magnetic domain reorientation that thereafter increases slowly up to saturation due to spin rotation. The hysteresis loops do not show any noticeable hysteresis effect. All samples exhibited low coercivity in the range of 10 to 81Oe values indicating that all the samples belong to the family of soft ferrites shown in Table 4.5. This magnetization process is connected with soft magnetic behavior of magnetic material. The slow process of magnetization toward the saturation value is connected with the magnetic anisotropy effect. Actual saturation could not be attained even with magnetic field as high as 10 kOe . From these $M - H$ loops at Figure 4.6, the remanence induction (M_r) and coercive force (H_c) were determined shows in Table 4.4.

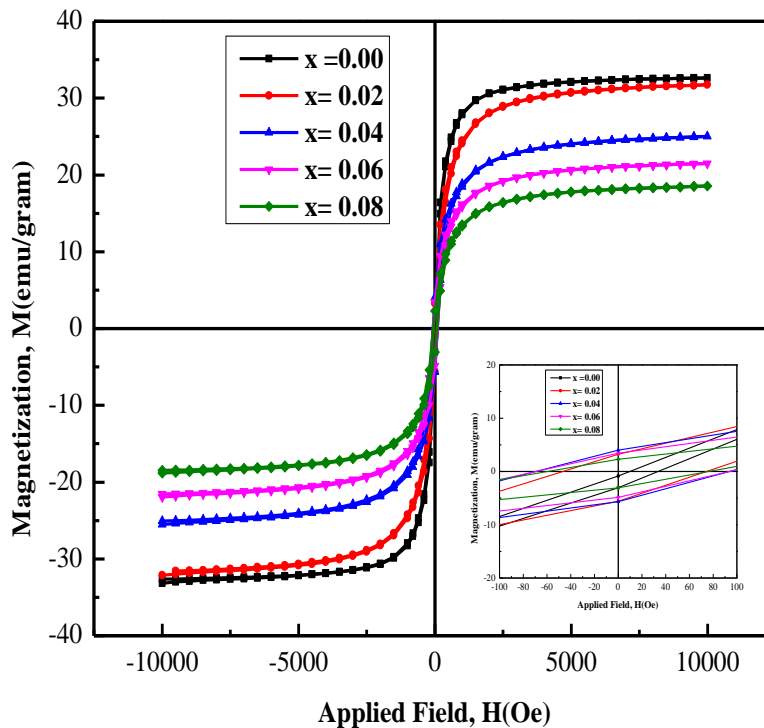


Figure 4.6: Hysteresis loops of $\text{Cu}_{0.15}\text{Zn}_{0.85}\text{La}_x\text{Fe}_{2-x}\text{O}_4$, [Where $x = 0.00, 0.02, 0.04, 0.06$ and 0.08] ferrites at room temperature 300K

The value of saturation magnetization (M_s) were found to be decreased with the increase of La^{3+} doped content for all the samples. All the M_s values of La doped composition lower than that of the undoped Cu-Zn ferrites. The might be due to the presence of higher quantity of nonmagnetic ferrite lattice by LaFeO_3 phase.

The magnetization of each composition depends on the distribution of Fe^{3+} ions between the two sub lattices A and B, where the Cu^{2+} , Zn^{2+} and La^{3+} ions are non magnetic. It is mentioned that CuFe_2O_4 and ZnFe_2O_4 ferrites are known as mixed ferrites, where Cu^{2+} ions are located on both sites, and Zn^{2+} ions are located on B-sites. The substitution will lead to decrease Fe^{3+} ions on the B-sites and consequently the magnetization of the B-sites will decrease. The cation distribution of La^{3+} replaces the magnetic ions Fe^{3+} from B-site but the difference between the A- and B-site moment's decreases indicates the possibility of a non-collinear spin canting effect in the system [Yafet and Kittel 1952, Geller 1969, Patten and Liu 1983]. The magnetization of the A-sites will increase according to the increase of the Fe^{3+} ions on A-sites. So the net magnetization has decreases accordingly increasing La-content substituted Cu-Zn ferrites.

Table 4.4: Saturation magnetization (M_s), coercivity (H_c) and remanent magnetization (M_r) of $\text{Cu}_{0.15}\text{Zn}_{0.85}\text{La}_x\text{Fe}_{2-x}\text{O}_4$, [where $x = 0.00, 0.02, 0.04, 0.06, \text{ and } 0.08$] ferrites sintered at 1150°C holding time 3hours

Content	M_s (emu/gm)	H_c (Oe)	M_r (emu/gm)
X= 0.00	32.5	10	0.8
X= 0.02	31.6	60	3.2
X= 0.04	24.9	81	3.8
X= 0.06	21.3	80	3.3
X= 0.08	18.4	67	2.2

The value of H_c and M_r of nominal composition at $x = 0.00$ has higher than that of the undoped La in Cu-Zn ferrites. This might be due to better density and higher permeability of the La-doped Cu-Zn ferrite. The H_c and M_r were found in Table 4.4 to be gradually increased with increasing up to $x = 0.04$ and $> x = 0.04$ decreases. These are reason movement of domain walls has more difficult and hence the H_c increases and decreases meaning which distinguish reversible and irreversible types of relaxation due La^{3+} ions. Irreversible type of relaxation is those are compared an atomic pair which corresponds to irreversible domain wall movements under external field.

4.3.2 Frequency Dependence of Complex Permeability

The permeability as dependent on frequency of a magnetic material is an important parameter from the application consideration such as insulator. The study of complex permeability is essential to understand the practical application range in ac field. The optimization of the dynamic properties such complex permeability in the high frequency range requires in the MHz range requires a precise knowledge of the magnetization mechanisms involved. Permeability measures the capacity of the substance to take magnetization. It is one of the most important parameter in evaluating the magnetic properties of a material. The magnetization mechanisms contributing to the complex permeability is given by $\mu = \mu' - i\mu''$, where μ' is the real permeability that describes the stored energy expressing the component of magnetic induction B in phase and μ'' is the imaginary part permeability that describes the dissipation of energy expressing the component of B 90° out of phase with the alternating magnetic field H.

The complex permeability (μ' and μ'') has been determined as a function of in the range 1 KHz to 120 MHz at room temperature. For all the samples of $\text{Cu}_{0.15}\text{Zn}_{0.85}\text{La}_x\text{Fe}_{2-x}\text{O}_4$ ferrites sintered at 1150°C holding time 3hours by using the conventional technique based on the determination of the complex impedance of circuit loaded with toroid shaped sample. With the help of Wayne Kerr Impedance Analyzer we collected 800 data point for initial permeability at different frequency range from 1 KHz to 120MHz. Figure 4.7 shows the variation of μ' with frequency of the system $\text{Cu}_{0.15}\text{Zn}_{0.85}\text{La}_x\text{Fe}_{2-x}\text{O}_4$ ferrites sintered at 1150°C holding time 3hours. Among these data some of the values of initial permeability at different frequency range are listed in Table 4.5. It is seen that μ' remains almost constant until very high frequency up to 60MHz and after than drops rapidly. The fairly constant μ' values within 10kHz to 10MHz wide range of frequency region are known as the zone of utility because it demonstrates the compositional stability and quality of the La doped prepared Cu-Zn ferrites. The slightly decrease in μ' at $x = 0.02$ to 0.08 is probably due to minor precipitation of secondary phase FeLaO_3 . The μ' in La doped Cu-Zn ferrite materials are also depend on many factors like reversible domain wall displacement, domain wall bulging as well as microstructural features, average grain size decreases, intergranular porosity, etc. [Smit and Wijn, 1959].

Table 4.5: Values of initial permeability at different frequency range for $\text{Cu}_{0.15}\text{Zn}_{0.85}\text{La}_x\text{Fe}_{2-x}\text{O}_4$, [Where $x=0.00, 0.02, 0.04, 0.06$ and 0.08] ferrites

Content	μ' at 100Hz	μ' at 10KHz	μ' at 100KHz	μ' at 1MHz	μ' at 10MHz	μ' at 100MHz
$x = 0.00$	14	15	15	15	14	13
$x = 0.02$	18	18	18	18	17	14
$x = 0.04$	14	14	14	14	14	13
$x = 0.06$	15	16	16	16	16	14
$x = 0.08$	15	16	16	16	16	14

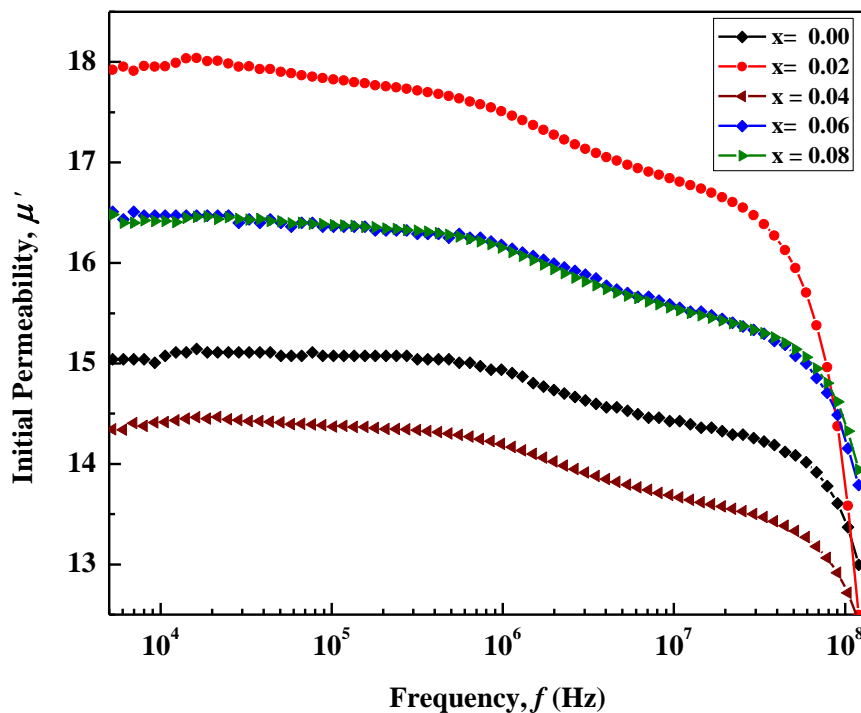


Figure 4.7: Frequency dependent initial permeability of $\text{Cu}_{0.15}\text{Zn}_{0.85}\text{La}_x\text{Fe}_{2-x}\text{O}_4$, [where $x=0.00, 0.02, 0.04, 0.06$ and 0.08] ferrites sintered at 1150°C for holding time 3 hours

For avoiding the noise peak we noticed that the real component of permeability μ' is fairly constant with frequency up to certain frequency range and then falls rather rapidly to very low value at higher frequency. Here the initial permeability remains stable for a long frequency range due to hopping of electron

between Fe^{2+} and Fe^{3+} . The permeability of composition with $x = 0.00$ to 0.08 were stable up to $1 - 10$ MHz and the cut off frequencies of samples were evident from these figures that the initial permeability as a function of frequency increases with Fe-deficiency (x -content), i.e. the permeability μ' is slightly increases with increases La content. The constant value of permeability over a wide frequency range, which is named the zone of utility of ferrites, is desirable over various applications such a broad band transformer and wide band read-writes head for video recording [Verma and Chatterjee 2006]. From Figure 4.7 the range of operating frequency up to 10MHz at constant permeability in the $x = 0.04$ and 0.06 samples are wider than that in the others which shows the compositional stability and quality of the ferrites samples. La^{3+} has no unpaired electrons and it behaves as diamagnetic. The substitution of ferromagnetic Fe^{3+} ($5\mu_B$) by diamagnetic La^{3+} in the spinel was not metal for increasing permeability. However, in the present case La^{3+} incorporation into the lattice is very small and hence slightly enhanced permeability with increasing La^{3+} ions due to its incorporation.

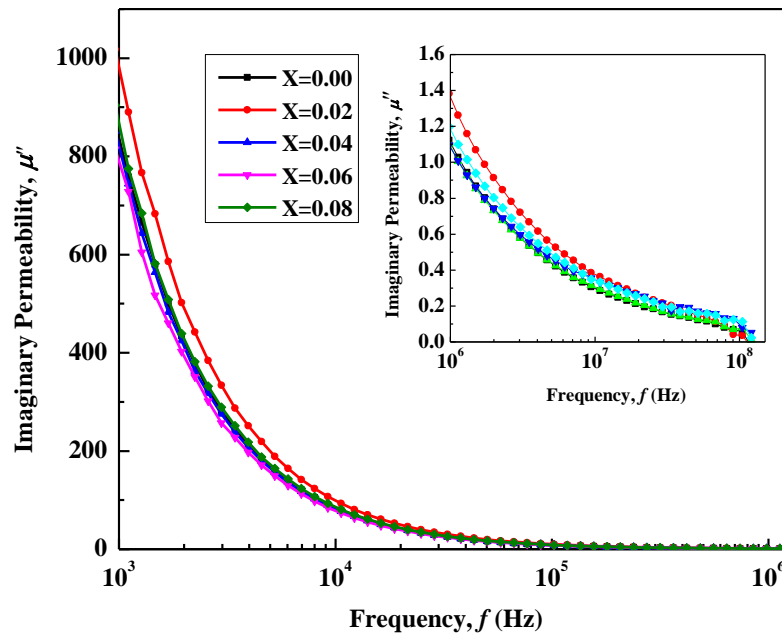


Figure 4.8: Frequency dependent imaginary permeability of $\text{Cu}_{0.15}\text{Zn}_{0.85}\text{La}_x\text{Fe}_{2-x}\text{O}_4$, [Where $x=0.00, 0.02, 0.04, 0.06$ and 0.08] ferrites sintered at 1150°C for 3 hours holding time.

The imaginary part of μ'' gradually decreased with the increased frequency and reached a minimum at a certain frequency, where the real part of permeability rapidly decreased as shown in Figure-4.8. From figure shows the μ'' initially high at low frequency zone all the La doped and undoped samples and then decreases with increasing frequency almost μ'' constant high frequency range. At high frequencies where the μ'' parameters become more significant, the inductors show high impedance and become resistive and dissipate interfering signals rather than reflecting these to the source [Snelling 1988]. When frequency is low, permeability is high and when frequency is high permeability is low. Thus, an effective limit of product of frequency and permeability is established. So, that effect of rare earth content of high frequency and high permeability are mutually incompatible.

4.3.2 Frequency Dependence of Quality Factor

Quality factor is an important parameter in a soft ferromagnetic material, since the amount of energy wasted on process other than magnetization can prevent the AC applications of a given material. The ratio of μ'' and μ' is equal $\tan\delta$ representing the losses in the material are a measure of the inefficiency of the magnetic system. The variation of loss factor, $\tan\delta$ ($= \mu''/\mu'$) with frequency for all samples has been studied. Figure 4.9 shows the variation of quality factor with frequency for various $\text{Cu}_{0.15}\text{Zn}_{0.85}\text{La}_x\text{Fe}_{2-x}\text{O}_4$, samples sintered at 1150°C holding time 3 hours. The magnetic losses, which cause the phase shift, can be split up into three components: hysteresis losses, eddy current losses and residual losses. This gives the formula $\tan\delta_m = \tan\delta_h + \tan\delta_e + \tan\delta_r$. As μ' is the initial permeability which is measured in presence of low applied magnetic field, therefore, hysteresis losses vanish at very low field strengths.

Figure 4.9 shows that clear value of $\tan\delta$ is less frequency dependent in the frequency range from $\geq 10\text{MHz}$. The loss is due to lag of domain wall motion with respect to the applied alternating magnetic field and is attributed to various domain defects [Shrotri *et. al.* 1999], which include non-uniform and non-repetitive domain wall motion, domain wall bowing, localized variation of flux density, nucleation and annihilation of domain walls. The low frequency dispersions are associated with domain wall dynamics [Gorter 1954] and high frequency to spin rotation. Both of these samples are shown here for a better understanding for the merit of the prepared materials for an induction device application. Cu-Zn-La ferrites have been found to

demonstrate reasonably good permeability at room temperature covering stable wide range of frequency can be used for MLCF application, such as embedded inductors or embedded capacitors. These mean that Cu-Zn-La ferrite materials are suitable for high frequency applications with high permeability.

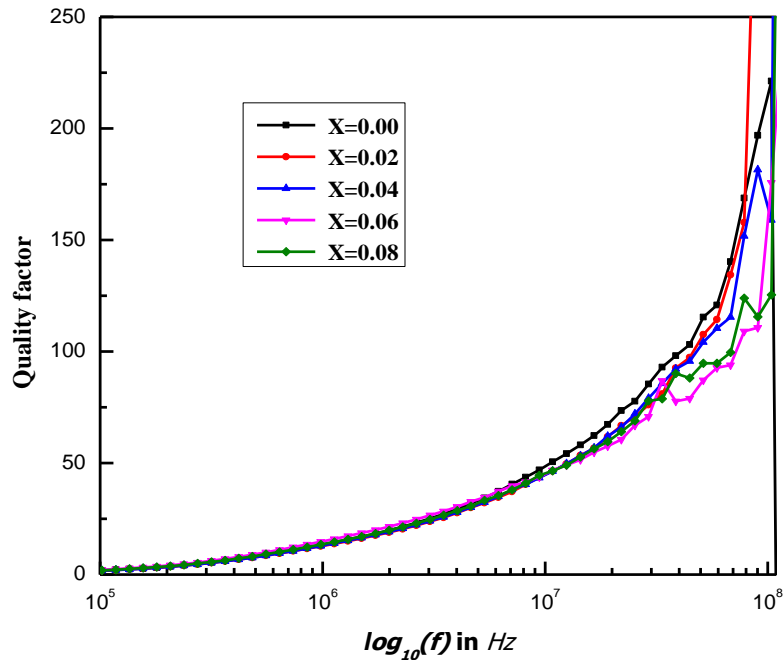


Figure 4.9: Frequency dependent loss factor of $\text{Cu}_{0.15}\text{Zn}_{0.85}\text{La}_x\text{Fe}_{2-x}\text{O}_4$, [Where $x=0.00, 0.02, 0.04, 0.06$ and 0.08] ferrites sintered at 1150°C for 3 hours

4.4 Frequency Dependent Dielectric Properties

Figure 4.10 shows the variation of dielectric constant, ϵ' with frequency for different composition of $\text{Cu}_{0.15}\text{Zn}_{0.85}\text{La}_x\text{Fe}_{2-x}\text{O}_4$ [Where $x=0.00, 0.02, 0.04, 0.06$ and 0.08] ferrites sintered at 1150°C holding time 3hours. Here the dielectric constant was measured over a wide range of frequency from 1 KHz to 120 MHz at room temperature. It can be seen from the figure the dielectric constant is found to decrease continuously with increasing frequency for all the specimens. The decrease in dielectric constant with increasing frequency is a normal behavior of ferrites. The dielectric dispersion is rapid at lower frequency region and it remains almost independent at high frequency side. The incorporation of rare earth elements La in Figure 4.10 into these ferrites has no pronounced effect on the dielectric constant in high frequency, but significantly decreases the dielectric constant in the low

frequency range. The type of behavior was observed in a number of ferrites such as Li- Co ferrites [Brockman *et. al.* 1950], Cu – Cd ferrites [Kolekar *et. al.* 1995], Ni– Cu–Zn ferrites [Khan *et. al.* 2013], Mg–Cu–Zn ferrites [Zhenxing Yue *et. al.* 2001, Bellad and Chougula 2000]. The dielectric behavior of ferrites may be explained on the basis of the mechanism of the dielectric polarization process and is similar to that of the conduction process. The electronic $Fe^{2+} \leftrightarrow Fe^{3+}$ gives the local displacement of electrons in the direction of applied electric field, which induces the polarization in ferrites [Zhenxing Yue *et. al.* 2001]. The La substituted Cu-Zn ferrites have high values of 3 to 40×10^3 at low frequencies.

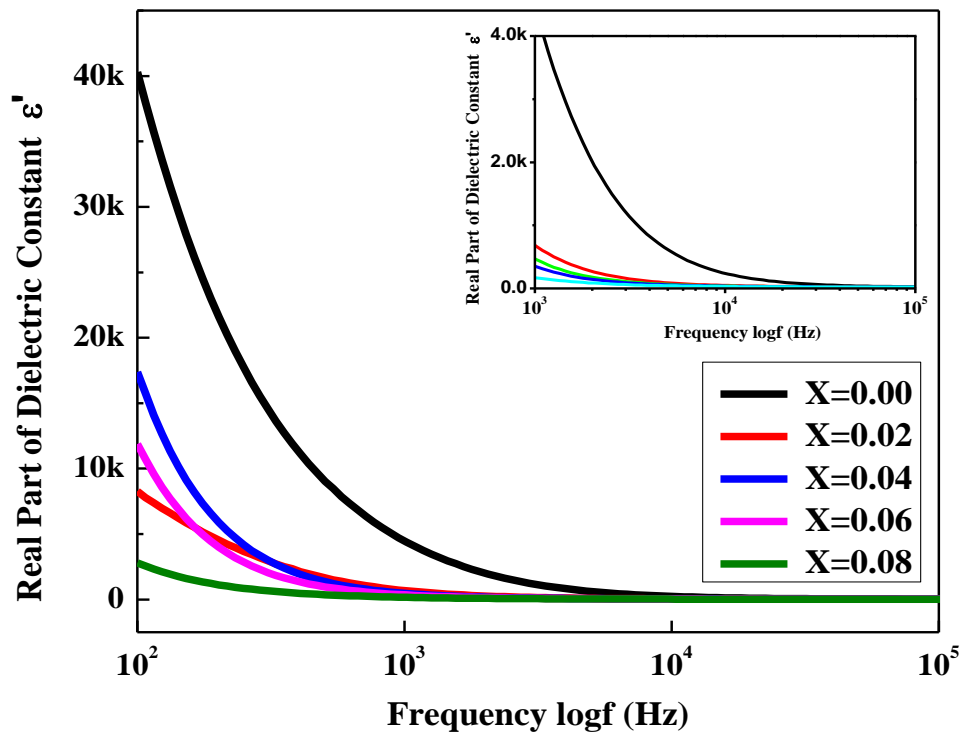


Figure 4.10: Frequency dependent real part of dielectric constant of $Cu_{0.15}Zn_{0.85}La_xFe_{2-x}O_4$, [Where $x=0.00, 0.02, 0.04, 0.06$ and 0.08] ferrites sintered at $1150^\circ C$ for holding time 3 hours

The imaginary part of dielectric constant, ϵ'' was also decreased with increasing frequency as shown in Figure 4.11. At very high frequency the value of ϵ'' becomes so small that it remains independent of applied frequency. The rapid decrease of ϵ'' at lower frequencies can also be explained on the basis of space charge polarization. We know that ferrites are made up of well conducting layer of grains

followed by poorly conducting layer of grain boundaries. During the exchange process between Fe^{3+} - Fe^{2+} the electrons have to pass through the grains and grain boundary of the dielectric medium. After that the electrons accumulate at grain boundary and produce space charge polarization.

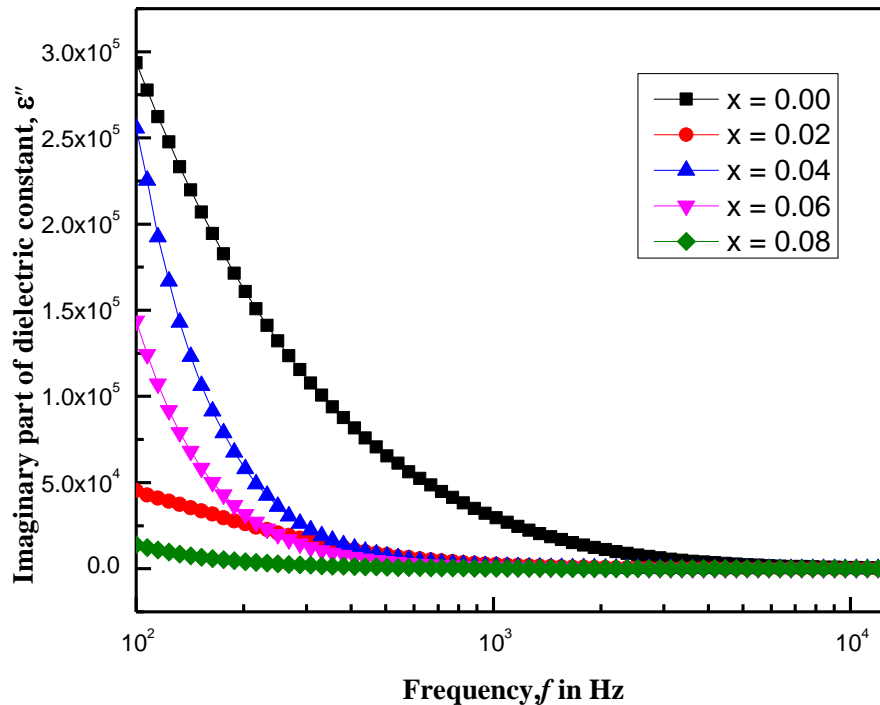


Figure 4.11: Frequency dependent imaginary part of dielectric constant of $\text{Cu}_{0.15}\text{Zn}_{0.85}\text{La}_x\text{Fe}_{2-x}\text{O}_4$, [Where $x=0.00, 0.02, 0.04, 0.06$ and 0.08] ferrites sintered at 1150°C for 3 hours

At low frequency the grain boundaries are more effective and at high frequency grains are effective [Ahmed *et. al.* 1989]. For this reason, grain boundary effect is responsible for decreasing imaginary part of the dielectric constant rapidly at low frequency region. At high frequency the polarization decreased, thus resulting in a decrease in imaginary part of the dielectric constant.

4.5 Effect of Lanthanum substitution on DC Resistivity

Resistivity is an important electrical property of ferrite materials. The electrical properties of ferrite materials depend upon the method of preparation, chemical

composition, grain size and sintering temperature. The variation of DC resistivity as a function of La content in Cu-Zn ferrites shows Figure 4.12. Figure shows electrical DC resistivity of the ferrite increases with increase in La content except to the sample for $x = 0.00$ for this reason higher resistivity compared to doped sample. It decreases with the increasing of La contents for $x = 0.02$ to 0.08 may be due to the decreases in grain size. Undoped sample is larger grains result in less number of grain boundaries which play as scattering centre for the flow of electrons and therefore decrease of resistivity as doped La content in Cu-Zn ferrites.

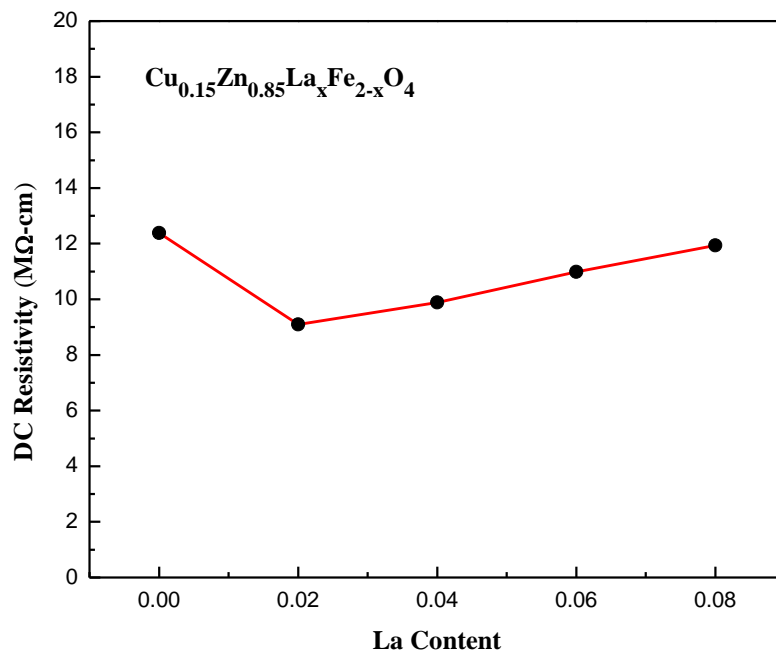


Figure 4.12: Variation of DC resistivity with La content (x) in $\text{Cu}_{0.15}\text{Zn}_{0.85}\text{La}_x\text{Fe}_{2-x}\text{O}_4$, [Where $x=0.00, 0.02, 0.04, 0.06$ and 0.08] ferrites sintered at 1150°C for 3 hours

The temperature dependence of DC electrical resistivity of $\text{Cu}_{0.15}\text{Zn}_{0.85}\text{La}_x\text{Fe}_{2-x}\text{O}_4$, ferrites sintered at $1150^\circ\text{C}/3\text{hrs}$ shown in Figure 4.13. Its electrical resistivity is at least a million times that of a metal. This very large resistivity means in turn that an applied alternating magnetic field will not induce eddy current in a ferrite. This property makes ferrite the best magnetic materials for high frequency applications where power losses from eddy currents must be minimized.

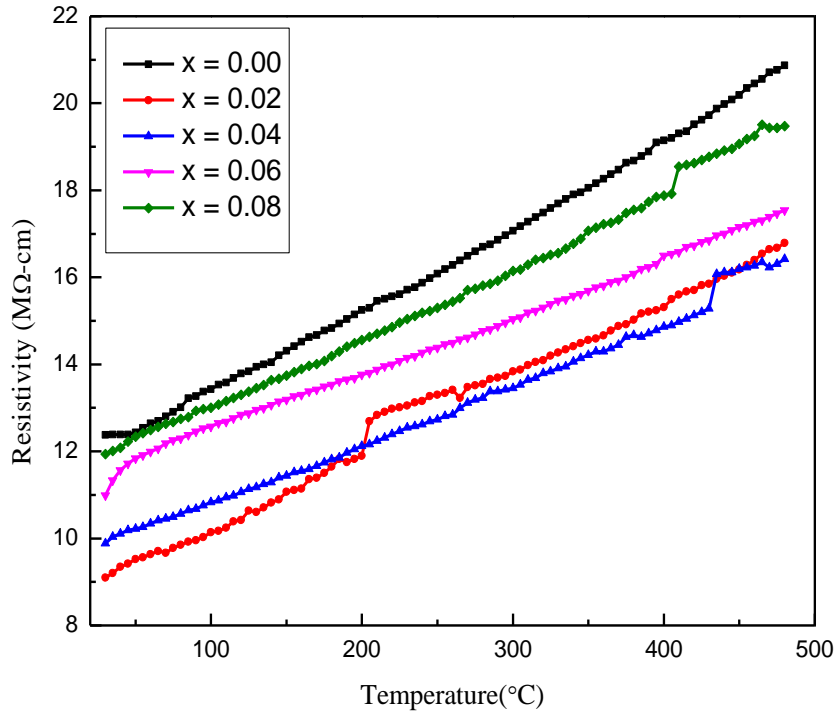


Figure 4.13: Temperature dependence DC resistivity of $\text{Cu}_{0.15}\text{Zn}_{0.85}\text{La}_x\text{Fe}_{2-x}\text{O}_4$, [where $x=0.00, 0.02, 0.04, 0.06$ and 0.08] ferrites sintered at 1150°C for holding time 3 hours

Ferrites of different compositions have been investigated. The above equation shows the variation of DC resistivity as a function of temperature shown in Figure 4.13. Electrical DC resistivity of ferrite increases with increasing temperature for all undoped and doped La content in Cu-Zn ferrites. The magnetic anisotropy field in ferrites results mainly from the presence of Fe^{2+} ions [Gorter 1954]. The anisotropy doped composition is lower than the undoped sample, i.e., Fe^{2+} ion concentration is lower for La doped composition.

CHAPTER V

CONCLUSIONS

CONCLUSIONS

5.1 Conclusions

The present work is focused on the synthesis, structural and detail study of electromagnetic properties of $\text{Cu}_{0.15}\text{Zn}_{0.85}\text{La}_x\text{Fe}_{2-x}\text{O}_4$ ferrites where $x = 0.00, 0.02, 0.04, 0.06$ and 0.08 samples are successfully made by the standard solid state reaction method. The powder samples were annealed at 850°C and pallet and ring shaped samples were sintered at 1150°C for holding time 3hours. Powdered samples had used in XRD, pallet were used for dielectric measurement, resistivity measurement and SEM analysis. Ring shaped sample were used for permeability and magnetization measurements.

- (i) The XRD patterns confirm the Cu-Zn ferrite is spinel cubic and Cu-Zn-La ferrites are pluriphasic (cubic and orthorhombic). The rare earth La substitution for Fe in the ferrite mainly produced secondary phase LaFeO_3 .
- (ii) The lattice parameter decreases initially La doped in Cu-Zn ferrites due to the replacement of Zn^{2+} ions (radius = 0.68\AA) by the larger La^{3+} ions (radius = 1.03\AA) in the octahedral sites. For this reason, the lattice parameter increases with the increase in La content in Cu-Zn ferrites, obeying the Vegard's law.
- (iii) The bulk density is lower than the actual X-ray density of the sample. Bulk density is decreasing slowly with increasing La content. The porosity of the samples increases with increasing La content whereas porosity follows the opposite trend with bulk density.
- (iv) SEM micrograph results indicate that the grain size of La doped in Cu-Zn ferrites has a significant effect on the grain growth of the sample and the grain size decreased with increases La content. Grain size has a great influence on the domain wall contribution hence on permeability. Average grain size is estimated in the range from 1600nm to 580nm .
- (v) The magnetization measurement has carried out by VSM. Saturation magnetization (M_s) decreases with increasing La content. All the M_s values of La doped composition lower than that of undoped Cu-Zn ferrites. This means due to presence of higher quantity of nonmagnetic ferrite lattice by LaFeO_3 phase. Coercivity was increased with La content up to $x = 0.06$ after increase La content decreases.

- (vi) Frequency dependent initial permeability remains almost constant until very high frequency up to 60MHz and then drops rapidly. The initial permeability is slightly increases with increasing La content whereas magnetic losses in association with loss tangent decreased.
- (vii) The imaginary permeability (μ'') initially high at low frequency zone all the La doped and undoped samples and then decreases with increasing frequency almost μ'' constant high frequency range. At high frequencies where the μ'' parameters become more significant, the inductors show high impedance and become resistive and dissipate interfering signals.
- (viii) The dielectric dispersion is rapid decreases at lower frequency region and it remains almost independent at high frequency side. The decrease in dielectric constant with increasing frequency is normal behavior. The effect La^{3+} ion into Cu-Zn ferrite has no pronounced effect of high frequency region but significantly decreases the dielectric constant in the low frequency region. The La substituted Cu-Zn ferrites have high values of 3 to 40×10^3 at low frequencies.
- (ix) The rapid decrease of imaginary part of dielectric constant at lower frequency range is basis of space charge polarization. During the exchange process between Fe^{3+} to Fe^{2+} the electrons have to pass through the grains and grain boundaries.
- (x) La free Cu-Zn ferrite lower than the La doped Cu-Zn ferrites may be due to the decreases in grain size. Undoped sample is larger grains result in less number of grain boundaries which play as scattering centre for the flow of electrons and therefore decrease of resistivity as doped La content in Cu-Zn ferrites. Electrical DC resistivity of ferrite increases with increasing temperature for all undoped and doped La content in Cu-Zn ferrites.

5.2 Scope for Future Work

With the development and advancement of Rare earth doped ferrites a tremendous surge in research on miniaturization and high frequency electronic devices is one rise soft magnetic materials are extensively used in inductors. This is the basic requirement in high frequency applications in technology areas. The following experiment and activities would be obtained as future work as the extension of this research.

- The characteristics in crystallization formation will be achieved by DSC thermal analysis.
- SEM can be studied for better understand surface nature and domain wall motion with substitution rear earth in ferrites shows biphasic microstructure constituted of matrix of dark grains and a second orthoferrite phase.
- Neutron diffraction analysis may be performed for these compositions to determine the distribution of substituted ions between A- and B- sites. Mössbauer spectroscopy can also be studied.
- The bond length and bonding mechanism would be carried out by FTIR spectroscopy.
- Some AC and DC electrical properties may be studied.
- Temperature dependent magnetization and dielectric properties will be carried out to understand the effect of temperature.

REFERENCES

REFERENCE

- Abbas T., Islam M. U. and Choudhury M. A. 1995: Study of sintering behavior and electrical properties of Cu-Zn-Fe-O system; *Modern Phys. Lett.*, B9, 1419 – 1426.
- Ahmed T. T., Rahman I. Z. and Tofial S. A. M 2004: Effect of Copper in distribution on the magnetization of nanoscaled Ni-Zn ferrites; *J. Magn. Magn. Matter*, 272 - 276, 2250 - 2252.
- Ahmed M., El Nimr. M., Tawfik A. and Aboel Ata A. 1989: Dialectical Behavior in Co-Zn ferrites; *Phys. Stat. sol. (a)*, Vol. 114, pp. 377 - 382.
- Ajmal M. and Maqsood A. 2008: Structural, electrical and magnetic properties of $\text{Cu}_{1-x}\text{Zn}_x\text{Fe}_2\text{O}_4$; *Journal of Alloys and Compounds*, 460, 54 – 59.
- Anderson P.W. 1963: In *Magnetism*; Vol 1, Eds, G. T. Rado and H. Shul; Academic Press, New York.
- Bahadur D., Giri J. Nayak B. B., Sriharsha T., Prasad N. K. 2005: Processing, Properties and Some Novel Applications of Magnetic Nanoparticles; *J. Pramana Phys.* 65, 663.
- Bellad S. S. and Chougula B. K 2000: Composition and frequency dependent dielectric properties of Li-Mg-Ti ferrites; *Matter S. Chem. Phys.*, 66,58.
- Bharathi K. K., Chelvane J. A., Markandeyulu G. 2009: Magnetoelectric properties of Gd and Nd-doped nickel ferrite; *J. Magn. Magn. Mater.* 321: 3677–3680.
- Bhaskar A., Rajini Kanth B. and Murthy S. R. 2004: Electrical properties of Mn added Mg-Cu- Zn ferrites prepared by microwave sintering method; *J. Magn. Magn. Mater.*, 283, 109.
- Brockman F. G., Dowling P. H. and Steneck W. G. 1950: Dimensional effects resulting from a high dielectric constant found in a ferromagnetic ferrite; *Phys. Rev.* 77, 85.
- Cullity B. D. 1959: *Elements of X-ray diffraction*; Addison-Wisley Pub., USA, 330.
- Dawoud H. and Shaat S. 2006: Magnetic properties of Zn substituted Cu ferrites; *An-Najah Univ. J. Res. (N. Sc.)*, 20, 87 – 100.
- Geller S. 1969: Comments on “Molecular-Field Theory for Randomly Substituted Ferromagnetic Garnet Systems” by I. Nowik”; *Phys. Rev.* 181, 980.

- Dai H., Li T.; Xue R.; Chen Z. 2012: Effects of Europium Substitution on the Microstructure and electric Properties of Bismuth Ferrite Ceramics; *J. Superconductor. Nov. Magn.* 25: 109-1154.
- Goldmann A. 1999: *Modern Ferrites Technology*; 2nd Edition, Pittsburgh, PA, USA.
- Gorter E. W. 1954: Saturation Magnetization and Crystal Chemistry of Ferrimagnetic Oxides; *Philips, Res. Rep.* 9, 295.
- Guo L., Shen X., Meng X., Feng Y. 2010: Effect of Sm³⁺ ions doping on structure and magnetic properties of nanocrystalline NiFe₂O₄ fibers; *J. Alloy. Compd.* 490 : 301–306.
- Hakim M. A., Manjurul Haque M., Huq M., Manjura Hoque Sk. and Norbblad P. 2000: Reentrant Spin Glass Behavior of Diluted Mg-Zn Ferrite; CP 1003, *Magnetic Materials International Conference on Magnetic Materials, AIP. P-295, ICMM – 2000.*
- Hakim M. A., Saha D. K. and Fazle Kibria A. K. M. 2007: Synthesis and temperature dependent structural study of nanocrystalline Mg-ferrite materials; *Bang. J. Phys.* 3, 57.
- Horvath M. P. 2000: Microwave applications of soft ferrites; *J. Magn. Magn. Mater.* 215 – 216, 171 – 183.
- Hossain M. A. 2017: Effect of Rare Earth Metal Substitution on the Structural, Magnetic and Transport Properties of Ni-Zn Ferrites; M. Phil Thesis; Khulna University of Engineering & Technology, Khulna 9203.
- Hossain M. A., Khan M. N. I. and Sikder S. S. 2017: Structural Magnetic and Dielectric Behaviors of Y³⁺ Substituted Ni-Zn Ferrites; *International Journal of Nano Science Trends and Technology*, Volume 1 Issue 2, p 1- 19.
- Hossain M. A., Khan M. N. I. and Sikder S. S. 2015: Effect of Resistivity, Permeability and Curie Temperature of Rare Earth Metal Europium (Eu) Substitution on Ni_{0.60}Zn_{0.40-x}Eu_xFe₂O₄ (x = 0.05, 0.10, 0.15) Ferrites; *ARPJN Journal of Science and Technology*, Vol.5, No.10, pp. 520 – 524.
- Jacobo S. E., Uhalde S. D., Bertorello H. R. 2004: Rare Earth influence on the structural and magnetic properties of Ni-Zn ferrites; *J. Magn. Magn. Mater.* **272**: 2253 - 2254.
- Jie S., Lixi W., Naicen X., Qitu Z. 2010: Introduction to Ferrite; *J. Rarte Earths*, 28, 445.

- Jing J., Liang-Chao L., Feng X. 2006: Preparation, Characterization and Magnetic Properties of PAN/La-substituted LiNi Ferrite Nanocomposites; *Chin. J. Chem.*, 24, 1804.
- Jing J., Liang-Chao L., Feng X. 2007: Structural Analysis and Magnetic Properties of Gd-Doped Li-ni Ferrites Prepared Using Rheological Phase Reaction Method; *J. Rare Earths* 25, 79.
- Khan Z. H., Mahbubur Rahman M., Sikder S. S., M. A. Hakim and D. K. Saha 2013: Complex Permeability of Fe deficient Ni-Cu-Zn ferrite; *Journal of Alloys and Compounds*, 548, 208 - 215.
- Khan Z. H., MahbuburRahman M., Sikder S. S. , Hakim M. A., ShireenAkhter, Das H. N. and Anjuman B. 2013: Thermal Hysteresis of Cu Substituted $\text{Ni}_{0.28}\text{Cu}_{0.10+x}\text{Zn}_{0.62-x}\text{Fe}_{1.98}\text{O}_4$ Ferrites; *Advanced Chemistry Letters*, 2, 1- 6.
- Kolekar C. B., Kamble P. N., Kulkarni S. G. and Vaingankar A. S.1995: Effect of Gd^{3+} substitution on dielectric behavior and copper-cadmium ferrites; *J. Matter. Sci.* 30, 5784.
- Kolekar C. B., Kamble P. N., Vaingankar A. S. 1995: Thermoelectric Power in Gd^{3+} substituted Cu-Cd Ferrites; *J. Bull. Mater. Sci.* 18(2), 133.
- Kong L. B., Li Z. W., Lin G. Q. and Gan Y. B. 2007: Magneto-dielectric properties of Mg-Cu-Co ferrite ceramics: II Electric, dielectric and magnetic properties; *J. An. Ceram. SOC* 90(7), 2104.
- Manjurul Huq M. and Huq M. and Hakim M. A. 2008: Thermal hysteresis of Permeability and Transport properties of Mn Substituted Mg-Cu-Zn ferrites; *Journal of Physics D: Applied Physics*, 41, 1 - 10.
- Manjurul Haque M., Huq M. and Hakim 2008: Influence of CuO and Sintering Temperature on the microstructure and magnetic properties of Mg-Cu-Zn ferrites; *J. Magn. Magn. Mater.*, 320, 2792 – 2799.
- Mendelson M. I. 1969: Average Grain Size in Polycrystalline Ceramics; *J. Am. Ceram. Soc.* 52, 8,443 - 446.
- Mondal P. K. 2018: Study of the Effect of Rare Earth Ions on the Structural, Magnetic and Electrical Properties of Cu-Zn Ferrites; M. Sc Thesis, Khulna University of Engineering & Technology, Khulna-9203.
- Neel L. 1948: Magnetic properties of Ferrites: Ferrimagnetisms and antiferromagnetism; *Anneals de Physics*, E3, 137-198.

- Nelson J. D. and Riely D. P. 1945: An experimental investigation of extrapolation methods in the derivation of accurate unit-cell dimensions of crystals; Proc. Phys. Soc. London 57, 160.
- Nikumbh A. K., Pawar R. A., Nighot D. V., Gugale G. S., Sangale M. D., Khanvilkar M. B., Nagawade A.V. 2014: Structural, electrical, magnetic and dielectric properties of rare-earth substituted cobalt ferrites nanoparticles synthesized by the co-precipitation method; J. Magn. Magn. Mater. 355 : 201–209.
- Ovidiu F. Caltun, Leonard Spinu July 2001: Magnetic properties of High frequency Ni-Zn Ferrites Doped with CuO; Trans. Magn. Vol.37, No.4,
- Patil R. S., Kakatkar S. V., Patil S. A., Maskar P. K. and Sawant S. R. 1991: Dielectric Behaviour of $\text{Li}_{0.5}\text{Zn}_x\text{Ti}_x\text{Fe}_{2.5-2x}\text{O}_4$ Ferrites; Phys. Status Solidi a 126 K185.
- Patton C. E. and Liu Y 1983: Localised canting models for substituted magnetic oxides; J. Phys. C: Solid State Phys. 16, 5995.
- Peng J., Hojamberdiev M., Xu Y., Cao B., Wang J., Wu H. 2011: Hydrothermal synthesis and magnetic properties of gadolinium-doped CoFe_2O_4 nanoparticles; J. Magn. Magn. Mater. 323: 133–137.
- Rana M. U., Islam M., Ahmad I. and Tahir Abbas 1998: Determination of magnetic properties and Y-K angles in Cu-Zn-Fe-O system; J. Magn. Magn. Mater., 187, 242.
- Roy P. K. and Bena J. 2009: Electromagnetic Properties of Samarium Substituted Ni-Cu-Zn Ferrite Prepared by Auto Combustion Method; J. Magn. Magn. Mater., 321(4), 247-251.
- Roess E. 1971: Ferrites; U. of Tokyo Press, Tokyo, Vol.5, p.187.
- Satter A. A. and El-Shokrofy K. M. 1997: Rare Earth Doping Effect on the Electrical Properties of Cu-Zn Ferrites; Physics IV CI, 245.
- Shahida Akhter, Paul D., Hakim, M. A., Saha, D., Al-Mamun A. and Perveen A. 2011: Synthesis, structural and physical properties of $\text{Cu}_{1-x}\text{Zn}_x\text{Fe}_2\text{O}_4$ ferrites; Mater. Sci. Appl., 2(11), 1675 – 1681.
- Shahida Akter, Md Abdul Hakim and Md Al-Mamun 2011: Synthesis, Structural and Physical Properties of $\text{Cu}_{1-x}\text{Zn}_x\text{Fe}_x\text{O}_4$ Ferrites; Mater. Scien. and Appl., 2, 1675 - 1681.

- Shrotri J. J., Kulkarni S. D., Deshpande C. E., Date S. K. 1999: Effect of Cu substitution on the magnetic and electrical properties of Ni-Zn ferrite synthesized by soft chemical method; *Mater. Chem. Phys.*, 59, 1.
- Smit J. and Wijn H. P. 1959: *Ferrites*; Philips Technical Library C Wiley, New York.
- Snelling E. C. 1988: *Soft Ferrites; Properties and Applications*; Ed., Butterworth, London.
- Snoek J. L. 1949: *New development in Ferromagnetism*; pp.139, Elsevier.
- Snoek J. L. 1984: *New development of Ferromagnetic Materials*; Elsevier Publ. Co. N.Y.
- Soilah Zahi, Mansor Hashim and Daud A. R. 2007: Synthesis, Magnetic and microstructure of Ni-Zn ferrite by Sol-gel technique; *J. Magn. Magn. Mater.* 308, 177.
- Vagards L., 1921: Die constitution der mischkristalle und die raumfullung der atome; *Z. Phys.* 5, 17.
- Vanuitert L. G.: High Resistivity Nickel Ferrites – the Effect of Minor Additions of Manganese or Cobalt; *J. Chem. Phys.* 23, 1883.
- Verway E. J. W. and Heilmann E. L. 1947: Physical properties and cation arrangement of oxides with spinel structures I. Cation arrangement in Spinel; *J. Chem. Phys.* 15(4), 181-187.
- Verma A. and Chatterjee R. 2006: Effect of zinc concentration on the structural, electrical and magnetic properties of mixed Mn-Zn and Ni-Zn ferrites synthesized by the citrate precursor technique; *J. Magn. Magn. Mater.* 306, 313 – 320.
- Virginia Fuentes, Aburto S. and Velenzuela R. 1987: Sub lattice in Nickel Ferrite; *J. Magn. Magn. Mater.*, 69, 233.
- William D. Callister 2003: *The University of Utah: Materials Science and Engineering* 6th Ed., Wiley.
- Yafet Y. and Kittel C. 1952: Antiferromagnetic arrangements in ferrites; *Phys. Rev.* 87, 290.
- Yan M. F. and Johnson D. W. 1978: Impurity induced exaggerated grain growth in Mn-Zn ferrites; *J. Am. Ceram. Soc.*, Vol. 61, No.7, pp.342.
- Yang Z. H., Gong Z., Q., Li H. X., Ma Y. T. and Yang Y. F. 2006: Synthesis of Ni-Zn Ferrites and Its Microstructure and Magnetic Properties; *Journal of Central South University of Technology*, 13, 618 - 623.

Yue Z., Zhou J., Li L. and Gui Z. 2001: Effects of MnO₂ on the electro-magnetic properties of Ni-Cu-Zn ferrites prepared by sol-gel auto combustion; J. Magn. Mater., 233, 224.

Zhenxing Yue, Zhou Ji, Longtu Li, Xiaolui Wang and Zhilun Gui 2001: Effect of copper on the electromagnetic properties of Mg-Zn-Cu ferrites prepared by Sol-gel auto-combustion method”; Mater. Sci. Eng. B 86, 64.

CONFERENCE PUBLICATIONS

1. **K. Nahar**, M. A. Hossain, M. N. I. Khan and S. S. Sikder; “Magnetic Complex Permeability of Lanthanum ions (La³⁺) Substituted Cu-Zn Ferrites”, International Conference on Physics 2018, 08-10 March, DU, Dhaka-1000, Bangladesh.
2. **K. Nahar**, M. A. Hossain, M. N. I. Khan and S. S. Sikder; “Investigation of the Magnetic and Transport Properties of Lanthanum (La) Substitution on Cu-Zn Ferrites”; Conference on Weather Forecasting and Advances in Physics, 11-12 May, 2018, KUET, Khulna-9203, Bangladesh.